A CONSTRAINED MOVING FINITE ELEMENT METHOD FOR MOVING BOUNDARY PROBLEMS

R. O. Moody

Numerical Analysis Report 10/87

UNIVERSITY OF READING

DEPARTMENT OF MATHEMATICS

P O BOX 220

READING RG6 2AX

Contents

Abstract

In this report we derive a one-dimensional finite element method on an adaptive mesh which is determined by the velocity of the moving boundary. A solution algorithm is presented and stability and truncation error analyses are carried out. Three test problems are described and the method, together with various special treatments, is applied to each. Numerical and graphical results are presented and analysed. A brief account is given of the extension of the method to two dimensions.

1. Introduction

Many physical processes, especially those concerned with heat flow and diffusion, may be described via moving boundary problems. Such problems differ from their fixed boundary relatives through the motion of one or more external boundaries. An additional condition is required at each moving boundary in order to determine the solution to the problem, which includes any moving boundary position.

One class of moving boundary problems concerned with melting and freezing contains the One- and Two-phase Stefan Problems, which are named after the early work of Stefan (1889a,b) and (1891). Another example of a moving boundary problem is the One-phase Oxygen Diffusion with Absorption Problem of Crank & Gupta (1972a,b).

Crank (1984) provides an extensive survey of the area of moving boundary problems, including numerical solutions of the above problems in both one and two dimensions. Numerical techniques have been employed on both the physical domain and on fixed domains obtained via a transformation. We describe some of these, concentrating on the one-dimensional case.

The coordinate transformation

$$\xi = x/s(t) \tag{1.1}$$

of Landau (1950) causes the variable one-dimensional

x-domain, [0,s(t)] (where s(t) denotes the position of the moving boundary at time t), to be mapped onto the time-invariant ξ-region, [0,1]. Nitsche (1980) implements (1.1) and a modified time variable, τ , given by

$$\tau = \int_0^t \frac{d\eta}{\{s(\eta)\}^2} , \qquad (1.2)$$

in his finite element solution of a one-dimensional One-phase Stefan Problem. Douglas & Gallie (1955) and Gupta & Kumar (1980) numerically solve a problem of this type using finite differences. Both sets of workers select time increments in order to ensure that the moving boundary is located at a grid point for each time level. Bonnerot & Jamet (1979) describe an implicit space-time biquadratic finite element method and implement it on a one-dimensional One-phase Stefan Problem. They prove their method to be third order accurate and illustrate its efficiency on problems with both continuous and discontinuous solutions.

Furzeland (1980) extends the domain-fixing idea of Landau (1950) for the case of the one-dimensional Two-phase Stefan Problem. Both the solid and liquid sub-regions are transformed onto the interval [0,1], and on each new domain the problem is discretised using the standard finite difference method with the theta implicit-explicit parameter. A novel transformation is present in the Isotherm Migration Method, in which the independent space coordinate and dependent temperature variable exchange roles to yield the

former as a function of the latter and time; namely,

$$x = x(u,t) \ . \tag{1.3}$$

This method was introduced by Chernousko (1970) and Dix & Cizek (1970) and is further implemented by Crank & Phahle (1973). Eyres, Hartree, Ingham, Jackson, Sarjant & Wagstaff (1946) proposed the use of an enthalpy variable: one which is representative of the total heat content. This choice of dependent variable forms the basis of the Enthalpy Method: a standard fixed-domain method which has been employed by many workers, including Bonacina, Comini, Fasano & Primicerio (1973), Atthey (1974), Voller & Cross (1981) and Bell (1982).

Ferriss & Hill (1974) solve the one-dimensional Oxygen Diffusion with Absorption Problem via an iterative finite difference technique on a fixed region, so obtained using (1.1). Crank & Gupta (1972a,b) make use of a short-time analytical solution and interpolation ideas in their finite difference solutions to this problem. The numerical solution of Hansen & Hougaard (1974) to this problem consists of an integral Equation formulation for the position of the moving boundary, and an integral formula for the dependent concentration variable. They solve the equation asymptotically for small times and apply a numerical technique to the latter. Miller, Morton & Baines (1978)

implement the analytic solution of Crank & Gupta (1972a,b) to begin their iterative finite element method. They use an adaptive mesh in which the number of nodes is automatically reduced in order to follow the inward motion of the boundary. The Local Moving Finite Element Method of Baines (1985) has been used by the author (1985) in his explicit solution of this problem.

In the present work we employ a constrained moving finite element method to the above problems, whose mathematical formulations are described in Section 2. In Section 3 we derive the adaptive method and describe its practical implementation. Also in this section we perform some theoretical analysis on the stability and truncation error of the method. A presentation of the solution algorithm, together with a brief account of the extension of the method to two dimensions, appears in Section 3. In Section 4 we describe certain special treatments necessary to each individual problem. Section 5 contains numerical and graphical results and discussion. Finally, in Section 6, we draw our conclusions.

2. The Test Problems

Here we briefly describe three moving boundary problems and present one-dimensional mathematical models thereof. These particular problems are selected in order to demonstrate the versatility of our adaptive mesh method which is outlined in detail in Section 3.

2.1 Problem 1 : The One-phase Stefan Problem

This problem is concerned with the melting of a semi-infinite block of ice via a prescribed temperature gradient at a fixed boundary. The position of the ice-water interface has to be determined in addition to the temperature in the water phase. Since the ice is assumed to be at its melting temperature, the solution in this region is not required. This problem was introduced by Hoffman (1977) and further studied by Furzeland (1980).

The mathematical formulation of an example of such a problem in non-dimensional variables is

$$u_t = u_{xx} , \qquad 0 < x < s(t) , \qquad t > 0 , \tag{2.1}$$

$$u_x = - \exp(t) , \qquad x = 0 , \qquad t > 0 , \tag{2.2}$$

$$\left.\begin{aligned} u &= 0 \\ u_x &= -\dot{s}(t) \end{aligned}\right\} , \quad x = s(t) , \qquad t > 0 , \tag{2.3}$$

$$u = 0 , \qquad 0 < x < s(0) \equiv 0 , \qquad t = 0 . \tag{2.4}$$

The above problem has an analytical solution of the form

$$\left.\begin{aligned} u &= \begin{cases} \exp(t-x) - 1 , & 0 < x < s(t) \\ 0 , & x > s(t) \end{cases} \\ s(t) &= t \end{aligned}\right\} , \quad t > 0 . \tag{2.5}$$

Numerical difficulties are apparent at time $t = 0$ since there is no water present. This is overcome by employing a short-time solution, details of which are presented in Section 4.1.

2.2 Problem 2 : The Two-phase Stefan Problem

The freezing of water into ice may be modelled via a Two-phase Stefan Problem. In this case the temperature in both the solid and liquid phases is to be determined as part of the solution, the remainder being the position of the ice-water interface as a function of time. The formulation below is an amended version of that presented by Ciavaldini (1975), and contains the classical explicit form of the moving interface velocity in terms of the jump in heat flux between the two phases. The model is

$$\left.\begin{aligned} u_t &= k_L \, u_{xx} + f_L(t) , \quad 0 < x < s(t) \\ u_t &= k_R \, u_{xx} + f_R(t) , \quad s(t) < x < 1 \end{aligned}\right\} , \quad 0 < t < t_1 , \tag{2.6}$$

$$\left.\begin{aligned} u_x &= 0 , \quad x = 0 \\ u_x &= 2 , \quad x = 1 \end{aligned}\right\} , \quad 0 < t < t_1 , \tag{2.7}$$

$$\left.\begin{aligned} u &= 0 \\ k_L\, u_x^- - k_R\, u_x^+ &= L\dot{s}(t) \end{aligned}\right\} , \quad x = s(t) , \quad 0 < t < t_1 , \tag{2.8}$$

$$u = x^2 - s_o^2 , \quad 0 < x < 1 , \quad t = 0 , \tag{2.9}$$

where

$$f_i(t) = -s_o^2 \exp(t) - 2k_i , \quad i = L , \quad R , \quad 0 < t < t_1 . \tag{2.10}$$

This apparently complex problem has a simple analytic solution of the form

$$\left.\begin{aligned} u &= x^2 - s_o^2 \exp(t) , \quad 0 < x < 1 \\ s(t) &= s_o \exp(\tfrac{1}{2}t) \end{aligned}\right\} , \quad 0 < t < t_1 , \tag{2.11}$$

where

$$\left.\begin{aligned} s_o &= s(0) \\ L &= 4(k_L - k_R) \\ t_1 &= -2\ln(s_o) \end{aligned}\right\} . \tag{2.12}$$

2.3 Problem 3 : The One-phase Oxygen Diffusion with Absorption Problem

In this problem of biological origin, oxygen diffuses into and is absorbed by tumour tissue until a steady state is attained. The oxygen in-flow boundary is then sealed, thus causing the gas content to be extracted by the continuing absorption process. The region in which oxygen is present therefore diminishes and eventually disappears. A non-dimensional mathematical formulation of the latter stage of this problem is

$$u_t = u_{xx} - 1 , \quad 0 < x < s(t) , \quad 0 < t < t_2 , \tag{2.13}$$

$$u_x = 0 , \quad x = 0 , \quad 0 < t < t_2 , \tag{2.14}$$

$$\left.\begin{aligned} u &= 0 \\ u_x &= 0 \end{aligned}\right\} , \quad x = s(t), \quad 0 < t < t_2 , \tag{2.15}$$

$$u = \tfrac{1}{2}(1-x)^2 , \quad 0 < x < s(0) \equiv 1 , \quad t = 0 . \tag{2.16}$$

The above formulation contains a derivative boundary condition, (2.14), which is inconsistent with the initial data, (2.16). Note also the lack of an explicit expression for the moving boundary velocity, thus rendering (2.13) -

(2.16) a problem of 'implicit' type. Although no analytical solution to the problem is known, numerical results have been produced by many workers, including Crank & Gupta (1972a,b), Ferriss & Hill (1974), Hansen & Hougaard (1974), Miller, Morton & Baines (1978) and Moody (1985).

3. The Numerical Method

In an earlier section we briefly outlined various domain-fixing and front-tracking methods which have been used to obtain numerical solutions of the three moving boundary problems of Section 2. Domain-fixing techniques, which can be easily implemented in one space dimension, do not readily generalise to higher dimensions, whereas front-tracking ones do. An example of such a method is the Moving Finite Element (MFE) Method of Miller & Miller (1981) and Miller (1981), which is further analysed by Wathen & Baines (1985). A local form of this technique (see Baines, 1985) has been implemented by the author (1985) in his numerical solution of the one-dimensional Oxygen Diffusion with Absorption Problem. Expressions are obtained for the nodal position velocities as well as the usual nodal amplitudal ones. One drawback with the explicit form of this method, however, is the requirement of very small time increments, especially in the later stages of the simulation when the length of the physical domain has become reduced, in order to prevent nodes from colliding with one another. The finite element method proposed here resembles that of the previous work, but is constrained so that the only nodal position velocity solved for is that at the moving boundary; the velocities of all interior nodes are specified proportionally between the fixed and moving boundaries. In the ensuing sections we derive the one-dimensional form of the method and discuss its implementation to Problems 1, 2 and 3.

3.1 Derivation of the Method

Consider a one-dimensional equation of the form

$$u_t = L(u) \ , \tag{3.1}$$

where L is a spatial differential operator. We seek a piecewise linear approximant, v, to the true solution, u, of the form

$$v = \sum_{j=1}^{N} a_j \alpha_j \ , \tag{3.2}$$

where $a_j = a_j(t)$, $j = 1(1)N$, are the amplitudal coefficients (or nodal values) at the corresponding nodal positions, $s_j = s_j(t)$, $j = 1(1)N$, collectively represented by the vector $\underline{s}(t)$, and $\alpha_j = \alpha_j(x, \underline{s}(t))$ are piecewise linear basis functions of local compact support. A typical interior α-type basis function is shown below in Figure 1.

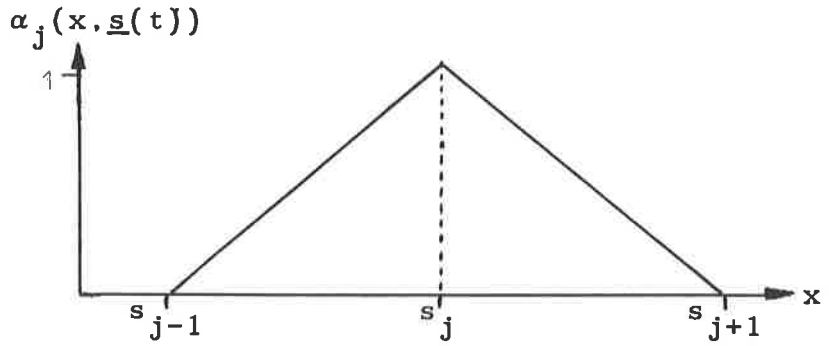

Figure 1

Differentiation of (3.2) with respect to time yields the expression

$$v_t = \sum_{j=1}^{N} \{\dot{a}_j \alpha_j + \dot{s}_j \beta_j\} \ . \qquad (3.3)$$

where $\beta_j = \beta_j(x, \underline{s}(t), \underline{a}(t))$, $j = 1(1)N$, are (in general) discontinuous piecewise linear basis functions (see Miller & Miller, 1981; Miller, 1981; and Wathen & Baines, 1983). It has been shown in Miller & Miller (1981) and Lynch (1982) that

$$\beta_j = -m\alpha_j \ , \qquad j = 1(1)N \ , \qquad (3.4)$$

where m is the local element slope of v . Figure 2 below depicts a typical interior β-type basis function.

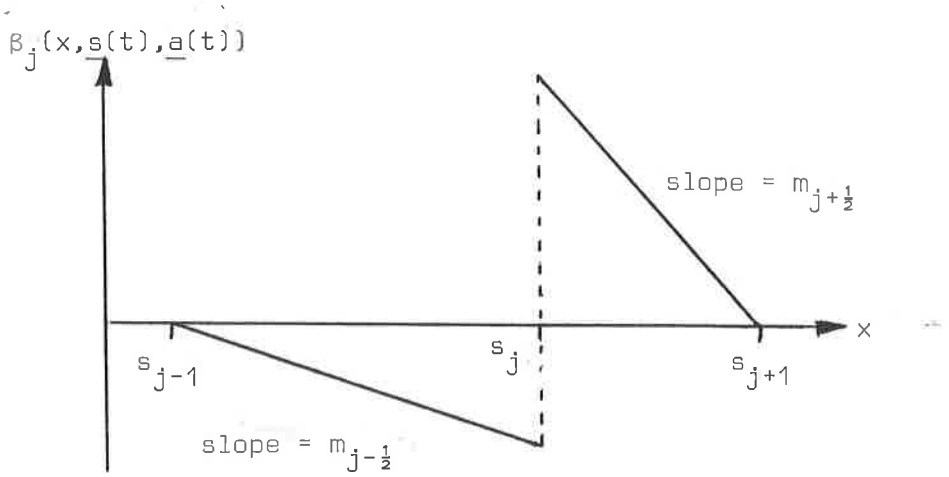

Figure 2

Minimisation of

$$||v_t - L(v)||_2^2 , \tag{3.5}$$

the global L_2 norm of the residual, over the variables $\dot{a}_j$, $j = 1(1)N$, taking $\dot{s}_j$, $j = 1(1)N$, to be parameters, gives rise to the Galerkin equations

$$\langle \alpha_i, v_t - L(v) \rangle = 0, \quad i = 1(1)N , \tag{3.6}$$

where $\langle \cdot, \cdot \rangle$ represents integration over the physical domain. Substitution of v_t from (3.3) into (3.6) produces the semi-discrete system of equations

$$\sum_{j=1}^{N} \{ \langle \alpha_i, \alpha_j \rangle \dot{a}_j + \langle \alpha_i, \beta_j \rangle \dot{s}_j - \langle \alpha_i, L(v) \rangle \} = 0 ,$$

$$i = 1(1)N . \tag{3.7}$$

We now determine the moving boundary velocity via its governing equation (details of the determination of which are given in Section 4 for each particular problem) and prescribe internal nodal velocities using the technique of Section

3.2.3. Implementation of (3.4) and an Euler time-stepping scheme with a θ implicit-explicit discretisation technique on the amplitudal velocities in (3.7) gives rise to a tridiagonal system of linear equations for the unknown amplitudes a_j , $j = 1(1)N$, at the next time level (for details see Section 3.2.3).

It is to be noted here that in the particular case of the One-phase Oxygen Diffusion with Absorption Problem an explicit expression for the moving boundary velocity does not appear. The value of the amplitude at the moving boundary, however, is known and is given by (2.15a). In this case we, therefore, minimise (3.5) over $\dot{a}_j$, $j = 1(1)N-1$ and $\dot{s}_N$, in order to provide an equation for the moving boundary velocity. (In one dimension the finite element equation for $\dot{s}_N$ is merely a multiple of that for $\dot{a}_N$.) We expand on this approach in Section 4.3.

3.2 Practical Implementation of the Method

We restrict our attention to operators L in Equation (3.1) of the form

$$L(u) = k\, u_{xx} + f(t) \ , \tag{3.8}$$

where k is the constant diffusivity of the fluid under consideration and f is a time-dependent forcing function. Included in this family of one-dimensional linear spatial differential operators are the three chosen test problems.

In the ensuing sections the finite element equations are presented together with the various numerical techniques employed in obtaining and solving for them.

3.2.1. Numerical Evaluation of Inner Products

Since the approximant is piecewise linear and second order spatial derivative terms are present in the governing Equation, these derivative terms cause the inner products to have the character of integrals of sums of delta functions. A technique to handle these inner products is required and we implement the approach of Mueller (1983) which is described below. The mollification method of Miller & Miller (1981) and Miller (1981) and the approach of Lynch (1982) yield identical values to those of Mueller (1983), as does the recovery idea in Johnson (1984) (see Morton, 1983).

Mueller's approach to the evaluation of $\langle \alpha_j, L(v) \rangle$ over the interval $[s_{j-1}, s_{j+1}]$ (which extends over the two elements $[s_{j-1}, s_j]$ and $[s_j, s_{j+1}]$) is as follows

(assuming a non-boundary element).

$$\langle \alpha_j, L(v) \rangle = \langle \alpha_j, k\, v_{xx} + f(t) \rangle$$

$$= k\langle \alpha_j, v_{xx} \rangle + \langle \alpha_j, f(t) \rangle$$

$$= k \int_{s_{j-1}}^{s_{j+1}} \alpha_j v_{xx} dx + \int_{s_{j-1}}^{s_{j+1}} \alpha_j f(t) dx$$

$$= k \int_{s_{j-1}}^{s_{j+1}} \{(\alpha_j v_x)_x - \alpha_{j,x} v_x\} dx + f(t) \int_{s_{j-1}}^{s_{j+1}} \alpha_j dx$$

$$= k \left\{ [\alpha_j v_x]_{s_{j-1}}^{s_{j+1}} - \int_{s_{j-1}}^{s_{j+1}} \alpha_{j,x} v_x dx \right\}$$

$$+ \tfrac{1}{2}(h_{j-\frac{1}{2}} + h_{j+\frac{1}{2}}) f(t)$$

$$= k \left\{ -\int_{s_{j-1}}^{s_j} \left[\frac{1}{h_{j-\frac{1}{2}}}\right] m_{j-\frac{1}{2}}\, dx - \int_{s_j}^{s_{j+1}} \left[-\frac{1}{h_{j+\frac{1}{2}}} \right] \right.$$

$$\left. m_{j+\frac{1}{2}} dx \right\} + \tfrac{1}{2}(h_{j-\frac{1}{2}} + h_{j+\frac{1}{2}}) f(t)$$

$$= k[m_{j+\frac{1}{2}} - m_{j-\frac{1}{2}}] + \tfrac{1}{2}(h_{j-\frac{1}{2}} + h_{j+\frac{1}{2}}) f(t) \,, \tag{3.9}$$

where

$$\left.\begin{aligned} h_j &= s_{j+\frac{1}{2}} - s_{j-\frac{1}{2}} \\ m_j &= (a_{j+\frac{1}{2}} - a_{j-\frac{1}{2}})/h_j \end{aligned}\right\} . \qquad (3.10)$$

Note that the $[\alpha_j v_x]_{s_{j-1}}^{s_{j+1}}$ term disappears owing to the basis function α_j being zero at the two limits, and that both v_x and $\alpha_{j,x}$ are piecewise constant over elements.

3.2.2 Imposition of Fixed Boundary Conditions

The three test problems of Section 2 contain fixed Neumann boundary conditions of the form

$$u_x = \gamma_1(t) , \qquad (3.11)$$

for some function γ (see Equations (2.2), (2.7) and (2.14)). We impose (3.11) in the usual way for finite elements; namely, by absorbing it into the weak form of the differential equation. Implementation of (3.11) at $x = 0$ causes (3.9) to become

$$\langle \alpha_1, L(v) \rangle = k[\gamma_1(t) - m_{\frac{3}{2}}] + \tfrac{1}{2} h_{\frac{3}{2}} f(t) . \qquad (3.12)$$

The standard method of imposing a Dirichlet condition of the form

$$u = \gamma_2(t) \ , \tag{3.13}$$

at a fixed boundary is to reduce the dimension of the space, replace the finite element equation by (3.13) and perform any necessary adjustment to dependent equations. In the Appendix, however, we outline a possible approach of imposing such conditions weakly.

3.2.3 Formation of the Discrete Equations

The local compact support property of the α- and β-type basis functions, together with (3.4) and (3.9), enables us to express (3.7) (for an internal node s_i) as

$$\tfrac{1}{6}h_{i-\frac{1}{2}}\dot{a}_{i-1} - \tfrac{1}{6}h_{i-\frac{1}{2}}m_{i-\frac{1}{2}}\dot{s}_{i-1} + \tfrac{1}{3}(h_{i-\frac{1}{2}} + h_{i+\frac{1}{2}})\dot{a}_i$$

$$- \tfrac{1}{3}(h_{i-\frac{1}{2}}m_{i-\frac{1}{2}} + h_{i+\frac{1}{2}}m_{i+\frac{1}{2}})\dot{s}_i + \tfrac{1}{6}h_{i+\frac{1}{2}}\dot{a}_{i+1} - \tfrac{1}{6}h_{i+\frac{1}{2}}m_{i+\frac{1}{2}}\dot{s}_{i+1}$$

$$= k[m_{i+\frac{1}{2}} - m_{i-\frac{1}{2}}] + \tfrac{1}{2}(h_{i-\frac{1}{2}} + h_{i+\frac{1}{2}})f(t) \ . \tag{3.14}$$

Multiplication of (3.14) by six and implementation of (3.10b) yields

$$h_{i-\frac{1}{2}}\dot{a}_{i-1} - (a_i - a_{i-1})\dot{s}_{i-1} + 2(h_{i-\frac{1}{2}} + h_{i+\frac{1}{2}})\dot{a}_i$$

$$- 2(a_{i+1} - a_{i-1})\dot{s}_i + h_{i+\frac{1}{2}}\dot{a}_{i+1} - (a_{i+1} - a_i)\dot{s}_{i+1}$$

$$= 6k[(a_{i+1} - a_i)/h_{i+\frac{1}{2}} - (a_i - a_{i-1})/h_{i-\frac{1}{2}}]$$

$$+ 3(h_{i-\frac{1}{2}} + h_{i+\frac{1}{2}})f(t) \ , \qquad (3.15)$$

which has the generic form

$$\Delta_s\dot{a} - \Delta_a\dot{s} = k\Delta_a/\Delta_s + \Delta_s f(t) \ , \qquad (3.16)$$

where a and s represent nodal values and positions respectively and Δ_a , Δ_s denote differences therein. We now perform a θ implicit-explicit splitting of (3.16) to yield

$$\Delta_s\dot{a} - [\theta\Delta_a^{n+1} + (1-\theta)\Delta_a^n]\dot{s} = k[\theta\Delta_a^{n+1} + (1-\theta)\Delta_a^n]/\Delta_s^n +$$

$$\Delta_s^n\,[\theta f^{n+1} + (1-\theta)f^n] \ , \qquad (3.17)$$

where the n superscript denotes evaluation at the time level which directly precedes the $n+1$ one. Note that all element lengths in (3.17) are considered explicitly. (A stability analysis of a θ implicit-explicit treatment of both amplitudes and element lengths did not produce an unconditionally stable scheme for as large a range of θ.)

The above procedure applied to (3.15), in addition to the Euler time-stepping scheme

$$\dot{a} \simeq [a^{n+1} - a^n]/\Delta t \ , \tag{3.18}$$

where Δt is the time increment, yields

$$\begin{aligned}
& a_{i-1}^{n+1}\{h_{i-\frac{1}{2}} + \theta\Delta t[2\dot{s}_i + \dot{s}_{i-1}] - 6k\theta\Delta t/h_{i-\frac{1}{2}}\} \\
& + a_i^{n+1}\{2[h_{i-\frac{1}{2}} + h_{i+\frac{1}{2}}] + \theta\Delta t[\dot{s}_{i+1} - \dot{s}_{i-1}] + \\
& \qquad 6k\theta\Delta t[1/h_{i-\frac{1}{2}} + 1/h_{i+\frac{1}{2}}]\} \\
& + a_{i+1}^{n+1}\{h_{i+\frac{1}{2}} - \theta\Delta t[2\dot{s}_i + \dot{s}_{i+1}] - 6k\theta\Delta t/h_{i+\frac{1}{2}}\} \\
& = a_{i-1}^{n}\{h_{i-\frac{1}{2}} - (1-\theta)\Delta t[2\dot{s}_i + \dot{s}_{i-1}] + 6k(1-\theta)\Delta t/h_{i-\frac{1}{2}}\} \\
& + a_i^{n}\{2[h_{i-\frac{1}{2}} + h_{i+\frac{1}{2}}] - (1-\theta)\Delta t[\dot{s}_{i+1} - \dot{s}_{i-1}] - \\
& \qquad 6k(1-\theta)\Delta t[1/h_{i-\frac{1}{2}} + 1/h_{i+\frac{1}{2}}]\} \\
& + a_{i+1}^{n}\{h_{i+\frac{1}{2}} + (1-\theta)\Delta t[2\dot{s}_i + \dot{s}_{i+1}] + 6k(1-\theta)\Delta t/h_{i+\frac{1}{2}}\} \\
& + 3\Delta t(h_{i-\frac{1}{2}} + h_{i+\frac{1}{2}})[\theta f^{n+1} + (1-\theta)f^n] \ ,
\end{aligned} \tag{3.19}$$

as the finite element equation for the i^{th} internal nodal amplitude. For convenience we have omitted the n superscript of the element lengths and have denoted $f(t)$ by f^n in (3.19). With reference to (3.19) we see that a tridiagonal system of linear equations for the unknowns is obtained. This system may be easily inverted at each time level using a standard tridiagonal matrix solver such as TRISOL. However, we note that the system is symmetric if and only if θ is zero.

We now describe in detail the procedure for determining the nodal velocities $\dot{s}_i$, $i = 1(1)N$, which are required in (3.19). A numerical estimate of the moving boundary or interface velocity may be obtained by considering a discretisation of its determining equation (for details of each individual problem see Section 4). With reference to Figure 3 below, the internal nodal velocities are prescribed as follows.

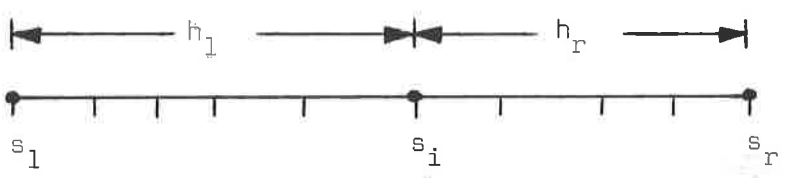

Figure 3

Suppose that s_l and s_r are boundary or interface nodes travelling with velocities $\dot{s}_l$ and $\dot{s}_r$ respectively and that s_i denotes the position of an internal node. In the case of Problems 1 and 3 and the solid region of Problem 2 we have

$$s_l = 0 \ , \quad s_r = s(t) \ , \quad \dot{s}_l = 0 \ , \quad \dot{s}_r = \dot{s}(t) \ , \tag{3.20a}$$

and in the liquid phase of Problem 2 these values are given by

$$s_l = s(t) \ , \quad s_r = 1 \ , \quad \dot{s}_l = \dot{s}(t) \ , \quad \dot{s}_r = 0 \ . \tag{3.20b}$$

The velocity of node i , $\dot{s}_i$, is assigned proportionally using

$$\begin{aligned} \dot{s}_i &= \dot{s}_l + h_l(\dot{s}_r - \dot{s}_l)/(h_l + h_r) \\ &= (h_r\dot{s}_l + h_l\dot{s}_r)/(h_l + h_r) \ . \end{aligned} \tag{3.21}$$

Techniques similar to the above for prescribing nodal motion appear in Murray & Landis (1959), O'Neill & Lynch (1981) and Lynch (1982).

We have now outlined the numerical techniques involved in the formation of the discrete equations at each time level, and in the next section we discuss the algorithm for obtaining approximate solutions to the three test problems.

3.2.4 The Numerical Solution Algorithm

In this section we present a simple solution algorithm and describe its implementation. Our five-step procedure for each time level is:-

(i) Obtain values of the external boundary (and interface) velocities.

(ii) Determine the velocities of all nodes, interior to either the domain or each sub-domain.

(iii) Form the system of equations for the nodal amplitudes of the subsequent time level.

(iv) Solve the above system for the new nodal values.

(v) Update the nodal positions.

The treatment required for Step (i) is particular to each individual problem and is therefore discussed separately in Section 4. Step (ii) is then carried out (using the relevant form of (3.20)) via Equation (3.21) of the previous section. The velocities of Step (ii) are then entered into (3.19) for each internal node. These equations, together with those from the fixed boundary (incorporating expressions of the form of (3.12)) and those from the moving boundary/interface (derived using further special treatments of Section 4) form the linear system of Step (iii). Step (iv) is performed using an efficient Gaussian elimination

algorithm suitable for tridiagonal systems, and (v) is carried out via the standard first-order Euler time-stepping scheme (see (3.18)).

3.2.5 Extension to Two Dimensions

In this section we outline the extension of the constrained method proposed here to two dimensions. As in the one-dimensional case we aim to obtain a piecewise linear approximating solution of the form of (3.2), but now with α-type basis functions which depend on both the horizontal and vertical nodal positions x_j , y_j , $j = 1(1)N$. An α-type basis function with 6 direct-neighbouring nodes is depicted below in Figure 4.

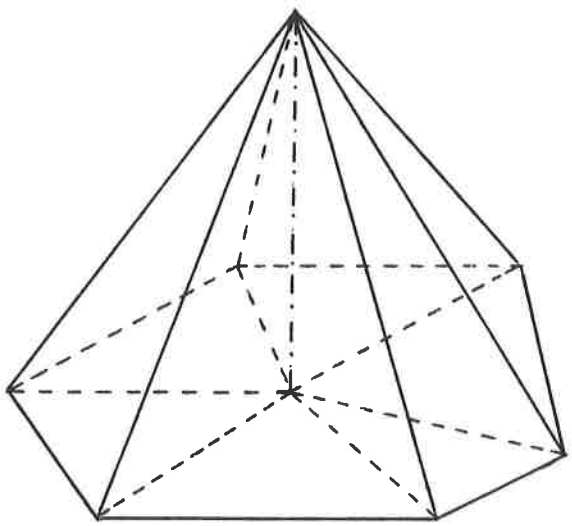

Figure 4

The time derivative of the approximant, v , assumes the form

$$v_t = \sum_{j=1}^{N} \{\dot{a}_j \alpha_j + (\dot{x}_j . \dot{y}_j) . \underline{\beta}_j\} \ . \qquad (3.22)$$

where

$$\underline{\beta}_j = (\beta_j , \gamma_j) \qquad (3.23)$$

is a vector of discontinuous basis functions. The result (3.4) now holds in the form

$$\beta_j = -m\alpha_j \ , \quad \gamma_j = -n\alpha_j \ , \qquad (3.24)$$

with m and n being the piecewise constant local element slopes in the horizontal and vertical directions respectively. In one dimension each slope has at most two components (since each node is surrounded by at most two elements, e_1 and e_2 say) , whereas the two-dimensional form may have many such components (see Figure 5).

One Dimension
(2 elements per node)

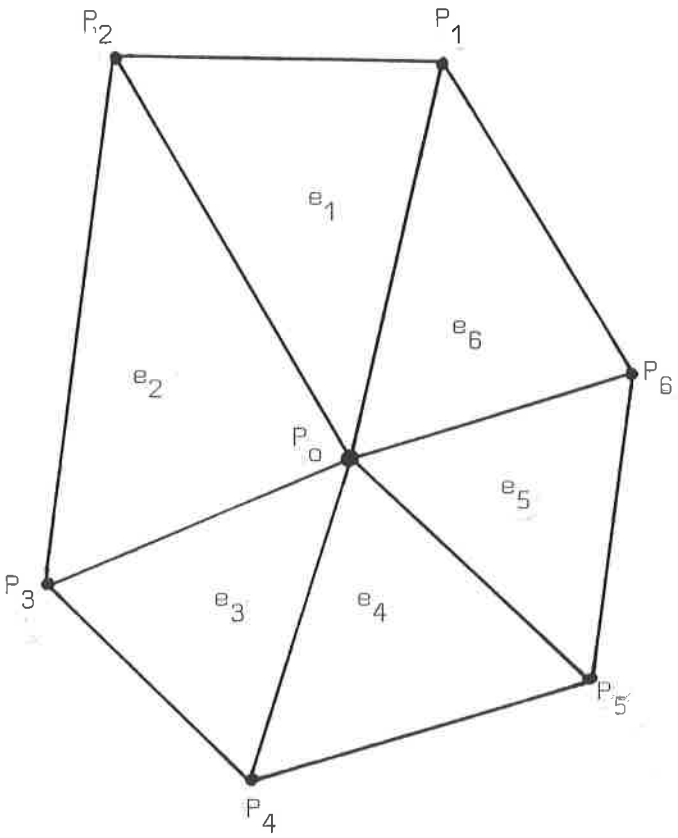

Two Dimensions
(typically 6 elements per node)

Figure 5

An identical minimisation of (3.5) over the same unknowns produces a system similar to (3.7); namely,

$$\sum_{j=1}^{N} \{\langle \alpha_i, \alpha_j \rangle \dot{a}_j + \langle \alpha_i, \beta_j \rangle \dot{x}_j + \langle \alpha_i, \gamma_j \rangle \dot{y}_j - \langle \alpha_i, L(v) \rangle\} = 0 \ ,$$

$$i = 1(1)N \ . \qquad (3.25)$$

As in the one-dimensional case, we discretise in space using a θ implicitness parameter and in time via the Euler formula. The resulting linear system, however, is neither tridiagonal nor symmetric and must therefore be inverted using a different technique, details of which will be presented in a later report, along with the specification of the nodal velocities.

We now briefly discuss the practical implementation of the method. The inner product evaluation technique of Mueller (1983) extends readily to two dimensions (see Johnson, 1985). Neumann and Dirichlet conditions at the fixed boundary may be imposed using the one-dimensional ideas of Section 3.2.2. We form the discrete finite element equations using the standard element-by-element assembly technique. With reference to Figure 5 we see that each triangular element contributes towards the equations of three unknown amplitudes. The two-dimensional form of Equation (3.14) is

$$\sum_{l\in e(i)} \{\tfrac{1}{12}\dot{J}_l\dot{a}_i - \tfrac{1}{12}J_lX_l\dot{x}_i - \tfrac{1}{12}J_lY_l\dot{y}_i\}$$

$$+ \sum_{j\in n(i)} \Big[\sum_{l\in e(i)\cap e(j)} \{\tfrac{1}{24}J_l\dot{a}_j - \tfrac{1}{24}J_lX_l\dot{x}_j - \tfrac{1}{24}J_lY_l\dot{y}_j\}\Big]$$

$$= k \sum_{l\in e(i)} \{\tfrac{1}{2}X_l\Delta y_{c(l)} - \tfrac{1}{2}Y_l\Delta x_{c(l)}\} + \tfrac{1}{6}\sum_{l\in e(i)} J_l f(t) \quad , \qquad (3.26)$$

where

$$\left.\begin{aligned} J_l &= \text{the Jacobian of element } l \\ X_l &= \text{the x-slope of element } l \\ Y_l &= \text{the y-slope of element } l \\ \Delta x_{c(l)} &= \text{a cyclic x-length in element } l \\ \Delta y_{c(l)} &= \text{a cyclic y-length in element } l \end{aligned}\right\} \quad , \qquad (3.27)$$

and $e(i)$, $n(i)$ are sets denoting the elements and nodes surrounding node i , respectively. The same treatment of the one-dimensional case applied to (3.27) produces an equation analagous to (3.19). Details will be presented in the later report.

The numerical solution algorithm of Section 3.2.4, incorporating special treatments (along the lines of those in Section 4), may also be easily implemented in the two-dimensional case.

3.3 Theoretical Analysis of the Method

In this section we perform some simple error and stability analysis on the general equation, (3.19), for internal nodes. For simplicity we restrict our attention to the case of equi-spaced nodes at each time level. Equation (3.19) with element lengths given by

$$h_i = h \ , \quad i = \tfrac{3}{2}(1)N-\tfrac{1}{2} \tag{3.28}$$

then becomes

$$\begin{aligned}
&a_{i-1}^{n+1}\{h + \theta\Delta t[2\dot{s}_{i-1} + \dot{s}_i] - 6k\theta\Delta t/h\} \\
&+ a_i^{n+1}\{4h + \theta\Delta t[\dot{s}_{i+1} - \dot{s}_{i-1}] + 12k\theta\Delta t/h\} \\
&+ a_{i+1}^{n+1}\{h - \theta\Delta t[2\dot{s}_i + \dot{s}_{i+1}] - 6k\theta\Delta t/h\} \\
&= a_{i-1}^{n}\{h - (1-\theta)\Delta t[2\dot{s}_{i-1} + \dot{s}_i] + 6k(1-\theta)\Delta t/h\} \\
&+ a_i^{n}\{4h - (1-\theta)\Delta t[\dot{s}_{i+1} - \dot{s}_{i-1}] - 12k(1-\theta)\Delta t/h\} \\
&+ a_{i+1}^{n}\{h + (1-\theta)\Delta t[2\dot{s}_i + \dot{s}_{i+1}] + 6k(1-\theta)\Delta t/h\} \\
&+ 6\ \Delta t\ h[\theta f^{n+1} + (1-\theta)f^n] \ .
\end{aligned} \tag{3.29}$$

The ensuing stability and local truncation error analysis is performed on Equation (3.29).

3.3.1 Stability Analysis

The stability of the proposed numerical scheme under the special case of zero forcing function is now investigated using the Fourier Method. It is, however, shown in Richtmyer & Morton (1967) that terms in the partial differential equation of lower order than the highest spatial derivative do not substantially affect the stability condition: a non-strict inequality is at most converted into a strict one.

Substitution of the Fourier mode

$$a_i^n = \kappa^n e^{i\iota\psi} \tag{3.30}$$

(where $\iota^2 = -1$), into (3.29) and division by a_i^n yields

$$\kappa = \kappa_n/\kappa_d \ , \tag{3.31}$$

where

$$\kappa_n = he^{-\iota\psi} - (1-\theta)\Delta t[2\dot{s}_i + \dot{s}_{i-1}]e^{-\iota\psi} + 6k(1-\theta)\Delta te^{-\iota\psi}/h$$

$$+ 4h - (1-\theta)\Delta t[\dot{s}_{i+1} - \dot{s}_{i-1}] - 12k(1-\theta)\Delta t/h$$

$$+ he^{\iota\psi} + (1-\theta)\Delta t[2\dot{s}_i + \dot{s}_{i+1}] + 6k(1-\theta)\Delta t e^{\iota\psi}/h \ , \quad (3.32a)$$

and

$$\kappa_d = he^{-\iota\psi} + \theta\Delta t[2\dot{s}_i + \dot{s}_{i-1}]e^{-\iota\psi} + 6k\theta\Delta t e^{-\iota\psi}/h$$

$$+ 4h + \theta\Delta t[\dot{s}_{i+1} - \dot{s}_{i-1}] + 12k\theta\Delta t/h$$

$$+ he^{\iota\psi} - \theta\Delta t[2\dot{s}_i + \dot{s}_{i+1}]e^{\iota\psi} - 6k\theta\Delta t e^{\iota\psi}/h \ . \quad (3.32b)$$

Using the relationships

$$\left.\begin{aligned} e^{\iota\psi} + e^{-\iota\psi} &= 4[\cos^2(\psi/2) - 1] \equiv 4[\hat{c}^2 - 1] \\ e^{\iota\psi} - e^{-\iota\psi} &= 4\iota\sin(\psi/2)\cos(\psi/2) \equiv 4\iota\hat{s}\hat{c} \end{aligned}\right\} \quad (3.33)$$

say, Equations (3.32) become

$$\left.\begin{aligned} \kappa_n &= A + B\hat{s}^2 + \iota D\hat{s}\hat{c} \\ \kappa_d &= A + E\hat{s}^2 - \iota F\hat{s}\hat{c} \end{aligned}\right\} , \quad (3.34)$$

where

$$\left.\begin{aligned} A &= 6h \\ B &= -4h - 24k(1-\theta)\Delta t/h - 2(1-\theta)\Delta t[\dot{s}_{i+1} - \dot{s}_{i-1}] \\ D &= 2(1-\theta)\Delta t[\dot{s}_{i-1} + 4\dot{s}_i + \dot{s}_{i+1}] \\ E &= -4h + 24k\theta\Delta t/h + 2\theta\Delta t[\dot{s}_{i+1} - \dot{s}_{i-1}] \\ F &= 2\theta\Delta t[\dot{s}_{i-1} + 4\dot{s}_i + \dot{s}_{i+1}] \end{aligned}\right\} . \quad (3.35)$$

The condition for stability is

$$|\kappa|^2 \leq 1 \ , \tag{3.36}$$

from which Equations (3.31)-(3.35) produce

$$G\hat{s}^2 \geq H \ , \tag{3.37}$$

with $\hat{s}$ defined in (3.33) and G and H by

$$\left.\begin{aligned} G &= E^2 - F^2 - B^2 + D^2 \\ H &= 2AB + D^2 - 2AE - F^2 \end{aligned}\right\} \ . \tag{3.38}$$

Since

$$0 \leq \hat{s}^2 \leq 1 \ , \tag{3.39}$$

the inequality (3.37) gives rise to the conditions

$$H \leq 0 \ , \quad H \leq G \ . \tag{3.40}$$

The first of (3.40) requires

$$\begin{aligned} &72k + 6h[\dot{s}_{i+1} - \dot{s}_{i-1}] + \\ &(2\theta - 1)\Delta t[s_{i-1} + 4\dot{s}_i + \dot{s}_{i+1}]^2 \geq 0 \ , \end{aligned} \tag{3.41}$$

and from the second the only meaningful conditions which arise are

$$\left.\begin{aligned} 12k + h[\dot{s}_{i+1} - \dot{s}_{i-1}] &\geq 0 \\ 2h^2 + (2\theta - 1)\Delta t\{12k + h[\dot{s}_{i+1} - \dot{s}_{i-1}]\} &\geq 0 \end{aligned}\right\} . \quad (3.42)$$

We see that if the first of (3.42), which is independent of the implicitness parameter θ, is satisfied then both (3.41) and (3.42b) hold for all $\theta \geq \frac{1}{2}$. For $\theta < \frac{1}{2}$ the time increment, Δt, must be restricted to satisfy

$$\Delta t \leq \min \{2h^2/[(1 - 2\theta)\Lambda] , \; 6\Lambda/[(1 - 2\theta)\{\dot{s}_{i-1} + 4\dot{s}_i + \dot{s}_{i+1}\}^2]\} , \quad (3.43)$$

for all subscripts, i, where

$$\Lambda = 12k + h[\dot{s}_{i+1} - \dot{s}_{i-1}] , \quad (3.44)$$

must be non-negative.

We now introduce the constrained nodal motion idea described by (3.21) into our stability analysis. Using the equi-spacing of nodes strategy (3.28) and the data (3.20a), (3.44) converts (3.42a) into

$$\Lambda = 6k + h^2\lambda \geq 0 \ , \tag{3.45}$$

where

$$\lambda = \dot{s}_N / s_N \ . \tag{3.46}$$

the numerical velocity per unit length. The denominator of the second argument of (3.43) is re-expressed as

$$36(1 - 2\theta)\dot{s}_N^{\,2}[s_i/s_N]^2 \ , \tag{3.47}$$

which is bounded above by

$$36(1 - 2\theta)\dot{s}_N^{\,2} \ . \tag{3.48}$$

We can therefore satisfy (3.43) by taking

$$\Delta t \leq \min \{2h^2/\Lambda \ , \ \tfrac{1}{6}\Lambda/\dot{s}_N^{\,2}\}/(1 - 2\theta) \ . \tag{3.49}$$

If (3.45) is satisfied the scheme is thus unconditionally stable for $\theta \geq \frac{1}{2}$; otherwise, Δt must satisfy (3.49).

We remark here that if $\lambda \geq 0$, then Λ remains non-negative. Condition (3.45) is always obeyed in our practical experience of the three test problems considered here and so does not invalidate Condition (3.49).

3.3.2 Local Truncation Error Analysis

The local truncation error, $\tau_i^{n+\theta}$, can be incorporated into the scheme via the replacement of the numerical amplitudes, a_i^n, by the true values, $u(s_i,n\Delta t)$, and the inclusion of the term

$$6h\Delta t\tau_i^{n+\theta} \quad . \tag{3.50}$$

in the right-hand side of (3.29). A rearrangement of the resulting equation yields

$$\begin{aligned}
&\tfrac{1}{6}\{[u(x_l,t') - u(x_l,t)] + 4[u(x_i,t') - u(x_i,t)] \\
&+ [u(x_r,t') - u(x_r,t)]\}/\Delta t - \tfrac{1}{6}\theta\{[u(x_i,t') - u(x_l,t')]\dot{s}^- \\
&+ 2[u(x_r,t') - u(x_l,t')]\dot{s} + [u(x_r,t') - u(x_i,t')]\dot{s}^+\}/h \\
&- \tfrac{1}{6}(1-\theta)\{[u(x_i,t) - u(x_l,t)]\dot{s}^- + 2[u(x_r,t) - u(x_l,t)]\dot{s} \\
&+ [u(x_r,t) - u(x_i,t)]\dot{s}^+\}/h = k\theta\{u(x_l,t') - 2u(x_i,t') \\
&+ u(x_r,t')\}/h^2 + k(1-\theta)\{u(x_l,t) - 2u(x_i,t) \\
&+ u(x_r,t)\}/h^2 + \{\theta f(t') + (1-\theta)f(t)\} + \tau_i^{n+\theta} \quad .
\end{aligned} \tag{3.51}$$

in which

$$t' = t + \Delta t \ , \tag{3.52}$$

and x_l , x_i , x_r denote the nodal positions s_{i-1} , s_i , s_{i+1} , moving with respective velocities $\dot{s}^-$, $\dot{s}$, $\dot{s}^+$. Taylor expansions of the terms in the left-hand side of (3.51) about the point (x_i, t) produce the following

$$\begin{aligned}
&u_\tau + \tfrac{1}{2}\Delta t u_{\tau\tau} + \tfrac{1}{6}h^2 u_{xx\tau} + \tfrac{1}{6}(\Delta t)^2 u_{\tau\tau\tau} \\
&- \tfrac{1}{6}\theta\{\dot{S}_1 u_x + \tfrac{1}{2}h\dot{S}_2 u_{xx} + \Delta t\dot{S}_1 u_{x\tau} + \tfrac{1}{6}h^2\dot{S}_1 u_{xxx} \\
&+ \tfrac{1}{2}h\Delta t\dot{S}_2 u_{xx\tau} + \tfrac{1}{2}(\Delta t)^2\dot{S}_1 u_{x\tau\tau}\} - \tfrac{1}{6}(1-\theta)\{\dot{S}_1 u_x \\
&+ \tfrac{1}{2}h\dot{S}_2 u_{xx} + \tfrac{1}{6}h^2\dot{S}_1 u_{xxx}\} + O[h^3] + O[h^2\Delta t] \\
&+ O[h(\Delta t)^2] + O[(\Delta t)^3] \ ,
\end{aligned} \tag{3.53}$$

where

$$\left.\begin{aligned}
\dot{S}_1 &= \dot{s}_l + 4\dot{s}_i + \dot{s}_r \\
\dot{S}_2 &= \dot{s}_r - \dot{s}_l
\end{aligned}\right\} \ . \tag{3.54}$$

and the τ derivative is a mobile one defined by by

$$u_\tau = u_t + \dot{s}u_x \ . \tag{3.55}$$

When the expressions of (3.54) are expanded in a similar manner, we obtain

$$\left.\begin{aligned} \dot{S}_1 &= 6\dot{s} + h^2\dot{s}_{xx} + O[h^4] \\ \dot{S}_2 &= 2h\dot{s}_x + \tfrac{1}{3}h^3\dot{s}_{xxx} + O[h^5] \end{aligned}\right\} \ . \tag{3.56}$$

Substitution of (3.56) into (3.53) yields

$$\begin{aligned} & u_\tau + \tfrac{1}{2}\Delta t u_{\tau\tau} + \tfrac{1}{6}h^2 u_{xx\tau} + \tfrac{1}{6}(\Delta t)^2 u_{\tau\tau\tau} \\ & - \theta\{\dot{s}u_x + \Delta t\dot{s}u_{x\tau} + \tfrac{1}{6}h^2[\dot{s}_{xx}u_x + \dot{s}_x u_{xx} + \dot{s}u_{xxx}] \\ & + \tfrac{1}{2}(\Delta t)^2\dot{s}u_{x\tau\tau}\} - (1-\theta)\{\dot{s}u_x + \tfrac{1}{6}h^2[\dot{s}_{xx}u_x \\ & + \dot{s}_x u_{xx} + \dot{s}u_{xxx}]\} + O[h^3] + O[h^2\Delta t] \\ & + O[h(\Delta t)^2] + O[(\Delta t)^3]. \end{aligned} \tag{3.57}$$

An identical treatment applied to the right-hand side of (3.51) produces

$$k\theta\{u_{xx} + \Delta t u_{xx\tau} + \tfrac{1}{12}h^2 u_{xxxx} + \tfrac{1}{2}(\Delta t)^2 u_{xx\tau\tau}\}$$

$$+ k(1-\theta)\{u_{xx} + \tfrac{1}{12}h^2 u_{xxxx}\} + \{f + \theta\Delta t\dot{f} +$$

$$\tfrac{1}{2}\theta(\Delta t)^2\ddot{f}\} + \tau_i^{n+\theta} + O[h^4] + O[h^2\Delta t] + O[(\Delta t)^3]. \quad (3.58)$$

From Equations (3.57) and (3.58) we obtain

$$\tau_i^{n+\theta} = \{u_\tau - \dot{s}u_x - ku_{xx} - f\} + \Delta t\{\tfrac{1}{2}u_{\tau\tau}$$

$$- \theta\dot{s}u_{x\tau} - k\theta u_{xx\tau} - \theta\dot{f}\} + h^2\{\tfrac{1}{6}u_{xx\tau}$$

$$- \tfrac{1}{6}\dot{s}_{xx}u_x - \tfrac{1}{6}\dot{s}_x u_{xx} - \tfrac{1}{6}\dot{s}u_{xxx} - \tfrac{1}{12}ku_{xxxx}\}$$

$$+ (\Delta t)^2\{\tfrac{1}{6}u_{\tau\tau\tau} - \tfrac{1}{2}\theta\dot{s}u_{x\tau\tau} - \tfrac{1}{2}k\theta u_{xx\tau\tau} - \tfrac{1}{2}\theta\ddot{f}\}$$

$$+ O[h^3] + O[h^2\Delta t] + O[h(\Delta t)^2] + O[(\Delta t)^3]\ . \quad (3.59)$$

Since u satisfies the partial differential equation

$$u_t = ku_{xx} + f\ , \quad (3.60)$$

(defined by (3.1) and (3.8)) and the mobile derivative form (3.55), we see that the first term of (3.59) disappears. We note also that if $\theta = \frac{1}{2}$ then the second term of (3.59) is a multiple of the time derivative of (3.60) and so this term vanishes as well. Since the third term of (3.59) is, in general, non-zero, we conclude that the local truncation error term for the $\theta \neq \frac{1}{2}$ case is of first order in time and second in space, whereas that for the $\theta = \frac{1}{2}$ case is second order, both in space and time. This result is identical to that of the θ method in finite differences.

4. Application of the Method to the Test Problems

In this section we describe the special treatments required for the individual test problems of Section 2. The common areas to be discussed are: initial placement of nodes, initial data representation, treatment at the moving boundary/interface and automatic selection of time increments.

We give here an outline of each of the above areas for the three test problems: further details are given in Sections 4.1-4.3. The nodes in Problems 1 and 3 are initially equi-spaced, whereas Problem 3 contains a small bunch of nodes at the moving interface. The initial amplitudes of Problems 2 and 3 are obtained via a least squares projection of the initial data functions (2.9) and (2.16), respectively. In Problem 1 we sample point values of a short-time solution at the nodal positions. All treatment at moving boundaries is based on the local recovery of the true solution via a least squares approach (see below). In all problems the time increment at each time level is chosen to obey the stability criterion of Section 3.3.1, while in Problem 3 it is further reduced in order to accommodate the large boundary velocity.

4.1 Special Treatment for Problem 1

The One-phase Stefan Problem, defined by equations

(2.1)-(2.4), presents us with an immediate difficulty: there is no liquid present initially and it is this phase which is of greatest interest. One possible remedy is to implement the analytic solution, (2.5), at a non-zero time as a start-up solution. A more general approach is as follows.

Substitution of $t = 0$ into (2.2) and (2.3b) yields

$$u_x = -1 \ , \quad \dot{s} = -u_x \ . \tag{4.1}$$

From this information we may deduce that the initial profile is approximately linear, with solution at time t_o (>0) given by

$$u = \begin{cases} t_o - x \ , & 0 < x < t_o \\ 0 \ , & x > t_o \end{cases} . \tag{4.2}$$

Note that (4.2) is the first term in the expansion of the analytic solution, (2.5). The difference, d, between the asymptotic and true solutions is such that

$$d = O[(x-t_o)^2] \ , \tag{4.3}$$

which assumes its maximum value, d_{max} , where

$$d_{max} = O[t_o^2] \ , \tag{4.4}$$

at $x = 0$. Thus if t_o is chosen to be small, then (4.2) is a reasonable approximation to (2.5a) at time t_o . In practice we choose

$$t_o = 0.01 \tag{4.5}$$

which gives

$$d_{max} = O[10^{-4}] \ . \tag{4.6}$$

The numerical initial data is provided by point values of (4.2) at equi-spaced nodes.

The Dirichlet Condition (2.3a) is replaced using an idea based on that of Miller, Morton and Baines (1978) which they apply to Problem 3. The presence of the two conditions (2.3) at the moving boundary suggests a locally quadratic solution q of the form

$$q(x) = Ax^2 + Bx + C \ , \tag{4.7}$$

where A,B,C are constant. The piecewise linear finite element solution in the rightmost element, $[s_{N-1},s_N]$, is given by

$$v(x) = \{a_{N-1}[s_N-x] + a_N[x-s_{N-1}]\}/[s_N-s_{N-1}] , \quad (4.8)$$

and is shown together with q in Figure 6.

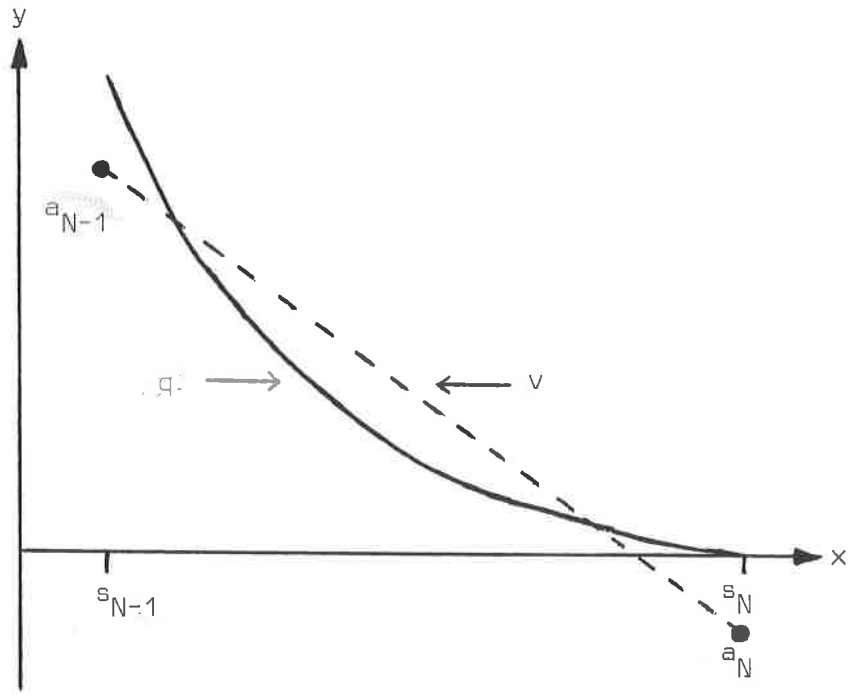

Figure 6

Minimisation of

$$S = \int_{s_{N-1}}^{s_N} \{q(x) - v(x)\}^2 dx \ , \tag{4.9}$$

over the variables a_{N-1}, a_N produces

$$\left.\begin{aligned} h^2_{N-\frac{1}{2}}A + 2h_{N-\frac{1}{2}}B + 6C &= 2a_{N-1} + 4a_N \\ 3h^2_{N-\frac{1}{2}}A + 4h_{N-\frac{1}{2}}B + 6C &= 4a_{N-1} + 2a_N \end{aligned}\right\} , \tag{4.10}$$

where $h_{N-\frac{1}{2}}$, the length of the last element, is defined by

$$h_{N-\frac{1}{2}} = s_N - s_{N-1} \ . \tag{4.11}$$

Imposition of the boundary conditions

$$\left.\begin{aligned} q(s_N) &= q_N \\ q^1(s_N) &= \tilde{q}_N \end{aligned}\right\} , \tag{4.12}$$

produces the relationship

$$a_{N-1} + 5a_N = 6q_N - h_{N-\frac{1}{2}}\tilde{q}_N \ . \tag{4.13}$$

Conditions (2.3) are implemented by

$$\left.\begin{aligned} q_N &= 0 \\ \tilde{q}_N &= -\dot{s}_N \end{aligned}\right\} , \tag{4.14}$$

to yield

$$a_{N-1} + 5a_N = h_{N-\frac{1}{2}}\dot{s}_N , \tag{4.15}$$

as a numerical representation of the Dirichlet Condition (2.3a).

We now describe the technique for determining the numerical moving boundary velocity $\dot{s}_N$, which depends on the gradient of the solution at the moving boundary (see equation (2.3b)). At each time level we have a finite element solution which is of the form of (4.8) in the element adjacent to the moving boundary. Suppose again, that the true solution is locally quadratic of the form of (4.7) and assumes the value q_N at $x = s_N$; i.e.

$$q(x) = A(x^2 - s_N^2) + B(x - s_N) + q_N . \tag{4.16}$$

If we now minimise (4.9) over A and B, then we obtain the explicit expression

$$q^1(s_N) = \{4q_N - a_{N-1} - 3a_N\}/h_{N-\frac{1}{2}} , \tag{4.17}$$

to represent the gradient of the true solution at the moving boundary. For this problem we have

$$q_N = 0 \ , \tag{4.18}$$

and so (4.17) becomes

$$q^1(s_N) = - \{a_{N-1} + 3a_N\}/h_{N-\frac{1}{2}} \ . \tag{4.19}$$

Condition (4.19) is implemented in (2.3b) to yield

$$\dot{s}_N^n = \{a_{N-1}^n + 3a_N^n\}/h_{N-\frac{1}{2}}^n \tag{4.20}$$

as the moving boundary velocity at time level n .

When the numerical scheme (3.19) is treated explicitly (i.e. with $\theta = 0$) , then (4.20) is in the correct form; otherwise it is not. An iteration or predictor-corrector technique may be used, but we shall implement the following idea. For a θ-scheme the required form of the moving boundary velocity is

$$\dot{s}_N^{n+\theta} = \dot{s}_N(t + \theta\Delta t) \ . \tag{4.21}$$

A Taylor series expansion of (4.21) yields

$$\dot{s}_N(t + \theta\Delta t) = \dot{s}_N(t) + \theta\Delta t\ddot{s}_N(t) + O[(\Delta t)^2] \ . \qquad (4.22)$$

The acceleration term $\ddot{s}_N$ of (4.22) can be manipulated to give

$$\ddot{s}_N = \dot{s}_N \frac{d\dot{s}_N}{ds_N} = (\dot{s}_N)^2/s_N \ . \qquad (4.23)$$

Substitution of (4.22) and (4.23) into (4.21) yields

$$\dot{s}_N^{n+\theta} = \dot{s}_N^n\{1 + \theta\Delta t\dot{s}_N^n/s_N^n\} \qquad (4.24)$$

as an accurate approximation to the numerical moving boundary velocity at time level $n + \theta$ in terms of the explicit one with $\theta = 0$.

In order to obtain an accurate representation of the true moving boundary velocity through (4.24), we maintain a small last element. At all time levels (including the first) nodes $N-1$ and N move with the velocity of the moving boundary (determined using (4.24)) and the constrained idea (3.21) is applied to the internal nodes s_i , $i = 2(1)N-2$.

The value for the time increment Δt at each time level is given by

$$\Delta t = \min\{\Delta t_s \ , \ \Delta t_{max}\} \ , \qquad (4.25)$$

for $0 \leq \theta < \frac{1}{2}$, where Δt_s satisfies the stability restriction (3.49), and is otherwise Δt_{max} , the maximum designated value of Δt .

4.2 Special Treatment for Problem 2

The Two-phase Stefan Problem considered here is defined by equations (2.6)-(2.10) and has an analytic solution given by (2.11).

Carey & Hung (1985) prove that the optimal nodal positions for piecewise linear approximants in the L_2 norm are obtained by equi-distribution of the modulus of the second derivative of the initial function raised to the power of two-fifths. Since the data (2.9) is quadratic, this approach suggests equi-spacing of nodes. In order to more accurately represent the piecewise linear approximant in the neighbourhood of the moving interface, we adopt the idea of Section 4.1 and choose the lengths of the elements to the immediate left and right of this interface to be small. So for given numbers N_L , N_R of interior nodes in the solid and liquid phases respectively, and left and right element lengths $h_{I-\frac{1}{2}}$, $h_{I+\frac{1}{2}}$ adjacent to the moving interface, the initial nodal positions are determined by (i) putting nodes at $x = 0$, $s(0)$, 1 , (ii) entering nodes at $s(0) - h_{I-\frac{1}{2}}$,

$s(0)+h_{I+\frac{1}{2}}$, where

$$0 < s(0) - h_{I-\frac{1}{2}} \ , \ s(0) + h_{I+\frac{1}{2}} < 1 \ , \tag{4.26a}$$

with

$$h_{I-\frac{1}{2}} = h_I/(N-1) = h_{I+\frac{1}{2}} \ , \ h_I = 10^{-2} \tag{4.26b}$$

(N being the total number of nodes), and (iii) equi-spacing N_L-1 nodes within the interval $[0,s(0)-h_{I-\frac{1}{2}}]$ and N_R-1 in $[s(0)+h_{I-\frac{1}{2}},1]$.

Having located the nodes, the initial amplitudes are then obtained by performing a least squares minimisation of

$$||u - v||_2^2 \ , \tag{4.27}$$

(with u and v defined in (2.9) and (3.2)) over the variables a_i , i = 1(1)N . This process produces an initial piecewise linear spline to represent the data (2.9).

We now extend the approach of Section 4.1 to obtain an amplitudal relationship which numerically represents Condition (2.8a). Again we assume locally quadratic behaviour, but now seek quadratics q_L , q_R in the elements $[s_{I-1},s_I]$, $[s_I,s_{I+1}]$ adjacent to the interface, s_I .

Figure 7 depicts the situation.

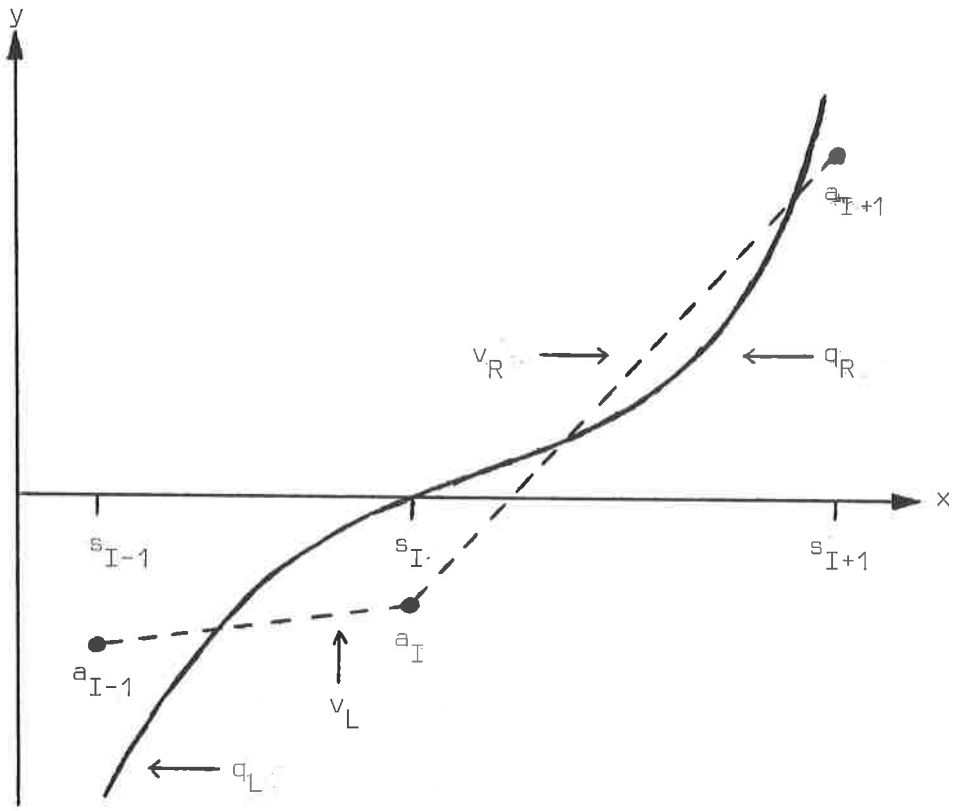

Figure 7

The functions q_L and q_R are defined by

$$\left.\begin{aligned} q_L(x) &= A_L x^2 + B_L x + C_L \\ q_R(x) &= A_R x^2 + B_R x + C_R \end{aligned}\right\}, \qquad (4.28)$$

and satisfy

$$\left.\begin{aligned} q_L(s_I) &= 0 = q_R(s_I) \\ k_L q_L^{\,1}(s_I) - k_R q_R^{\,1}(s_I) &= L\dot{s}(t) \end{aligned}\right\} , \tag{4.29}$$

in order to model Conditions (2.8). Minimisation of

$$S_L = \int_{s_{I-1}}^{s_I} \{q_L(x) - v_L(x)\}^2 dx , \tag{4.30}$$

over a_L, a_I and of

$$S_R = \int_{s_I}^{s_{I+1}} \{q_R(x) - v_R(x)\}^2 dx , \tag{4.31}$$

over a_I , a_R produces four linear equations, which together with (4.29) yield a system of seven equations in the seven unknowns A_L, B_L, C_L, A_R, B_R, C_R and a_I . The resulting relationship between the numerical interface value and its adjacent amplitudes is

$$\begin{aligned} &(k_L/h_{I-\frac{1}{2}})a_{I-1} + 5[(k_L/h_{I-\frac{1}{2}}) + (k_R/h_{I-\frac{1}{2}})]a_I + (k_R/h_{I+\frac{1}{2}})a_{I+1} \\ &\qquad = - L\dot{s}_I , \end{aligned} \tag{4.32}$$

with the interface velocity $\dot{s}_I$ being supplied using the technique described below.

A minor extension of the slope recovery idea, defined through equations (4.16)-(4.19) in Section 4.1, produces

$$\left.\begin{aligned} q^1{}_L(s_I) &= -\{a_{I-1} + 3a_I\}/h_{I-\frac{1}{2}} \\ q^1_R(s_I) &= \{3a_I + a_{I+1}\}/h_{I+\frac{1}{2}} \end{aligned}\right\} . \qquad (4.33)$$

An explicit discretisation of (2.8b) can be obtained by replacing u_x^- , u_x^+ therein by q_L , q_R , respectively, of (4.33) to give

$$k_L q^1{}_L(s_I) - k_R q^1{}_R(s_I) = L\dot{s}_I . \qquad (4.34)$$

which can be rearranged to yield

$$\dot{s}_I = -\{k_L[a_{I-1}+3a_I]/h_{I-\frac{1}{2}} + k_R[3a_I+a_{I+1}]/h_{I+\frac{1}{2}}\}/L . \qquad (4.35)$$

The extrapolation technique (4.21)-(4.23) is then applied to (4.35) to produce

$$\dot{s}_I^{n+\theta} = \dot{s}_I^n\{1 + \theta\Delta t\dot{s}_I^n/s_I^n\} , \qquad (4.36)$$

where

$$\begin{aligned} \dot{s}_I^n = -\{&(k_L/h^n_{I-\frac{1}{2}})a^n_{I-1} + 3[(k_L/h^n_{I-\frac{1}{2}}) + (k_R/h^n_{I+\frac{1}{2}})]a^n_I \\ &+ (k_R/h^n_{I+\frac{1}{2}})a^n_{I+1}\} . \end{aligned} \qquad (4.37)$$

Equation (4.25), as in the case of the One-phase Stefan Problem, defines the stability restriction for $0 \leq \theta < 1$ on the time increment at each time level; for $\theta \geq \frac{1}{2}$ we, again, use Δt_{max}.

4.3 Special Treatment for Problem 3

The initial amplitudes for the One-phase Oxygen Diffusion with Absorption Problem, (2.13)-(2.16), at the equi-spaced nodes are determined by minimising (4.27) over these variables: this is identical to the approach of Section 4.2, but with (2.16) instead of (2.9).

We again impose the Dirichlet condition (2.15a) via consideration of a quadratic form (4.7) of the true solution in the neighbourhood of the moving boundary. Equations (4.8)-(4.12) yield (4.13), in which we set

$$\left.\begin{aligned} q_N &= 0 \\ \tilde{q}_N &= 0 \end{aligned}\right\} , \tag{4.38}$$

to produce the result of Miller, Morton & Baines (1978)

$$a_{N-1} + 5a_N = 0 , \tag{4.39}$$

to numerically represent (2.15a).

We now explain the determination of the numerical moving

boundary velocity $\dot{s}_N$, and hence the nodal amplitudes at the new time level. The finite element equation for $\dot{s}_N$, obtained by minimising (3.5) with L defined by

$$L(v) = v_{xx} - 1 \ , \tag{4.40}$$

either over $\dot{s}_N$ and scaling by $-1/m_{N-\frac{1}{2}}$ or over $\dot{a}_N$, is

$$\begin{aligned} &\tfrac{1}{6}h_{N-\frac{1}{2}}\dot{a}_{N-1} - \tfrac{1}{6}h_{N-\frac{1}{2}}m_{N-\frac{1}{2}}\dot{s}_{N-1} + \tfrac{1}{3}h_{N-\frac{1}{2}}\dot{a}_N \\ &- \tfrac{1}{3}h_{N-\frac{1}{2}}m_{N-\frac{1}{2}}\dot{s}_N = - m_{N-\frac{1}{2}} - \tfrac{1}{2}h_{N-\frac{1}{2}} \ , \end{aligned} \tag{4.41}$$

where $h_{N-\frac{1}{2}}$, $m_{N-\frac{1}{2}}$ are as defined in (3.10). The θ implicit-explicit discretisation technique of Section 3.2.3 converts (4.41) into an equation of the form

$$F(\dot{s}_N^{n+\theta} \ ; \ \dot{s}_{N-1}^{n+\theta} \ ; \ \Delta t \ , \ h_{N-\frac{1}{2}}^n \ , \ a_{N-1}^n \ , \ a_N^n \ , \ a_{N-1}^{n+1} \ , \ a_N^{n+1}) = 0 \ , \tag{4.42}$$

where

$$\begin{aligned} F = \ & h_{N-\frac{1}{2}}^n\{a_{N-1}^{n+1} - a_{N-1}^n + 2[a_N^{n+1} - a_N^n] + 3\Delta t\} \\ & - \Delta t\{\theta[a_N^{n+1} - a_{N-1}^{n+1}] + (1-\theta)[a_N^n - a_{N-1}^n]\}[\dot{s}_{N-1}^{n+\theta} + 2\dot{s}_N^{n+\theta}] \\ & + 6\Delta t\{\theta[a_N^{n+1} - a_{N-1}^{n+1}] + (1-\theta)[a_N^n - a_{N-1}^n]\}/h_{N-\frac{1}{2}}^n \ . \end{aligned} \tag{4.43}$$

Equation (4.43) may be expressed in the form

$$F = A - B[\dot{s}_{N-1}^{n+\theta} + 2\dot{s}_{N}^{n+\theta}] + C \ , \tag{4.44}$$

in which

$$\left.\begin{aligned} A &= h_{N-\frac{1}{2}}^{n}\{a_{N-1}^{n+1} - a_{N-1}^{n} + 2[a_{N}^{n+1} - a_{N}^{n}] + 3\Delta t\} \\ B &= \Delta t\{\theta[a_{N}^{n+1} - a_{N-1}^{n+1}] + (1-\theta)[a_{N}^{n} - a_{N-1}^{n}]\} \\ C &= 6\Delta t\{\theta[a_{N}^{n+1} - a_{N-1}^{n+1}] + (1-\theta)[a_{N}^{n} - a_{N-1}^{n}]\}/h_{N-\frac{1}{2}}^{n} \end{aligned}\right\} \ . \tag{4.45}$$

The prescribed nodal motion idea, (3.21), produces

$$\dot{s}_{N-1}^{n+\theta} = [(N-2)/(N-1)]\dot{s}_{N}^{n+\theta} \ , \tag{4.46}$$

which when substituted into (4.44) yields

$$F = A - D\dot{s}_{N}^{n+\theta} + C \ , \tag{4.47}$$

where

$$D = B[3 - 1/(N-1)] \ . \tag{4.48}$$

We can therefore determine the moving boundary velocity using

$$\dot{s}_{N}^{n+\theta} = (A + C)/D \ , \tag{4.49}$$

provided that the values a_{N-1}^{n+1} , a_N^{n+1} at the new time level are known.

The above working suggests an iteration algorithm in which the following is considered at each time level $n \geq 0$.

(i) Estimate $(\dot{s}_N^{n+\theta})_o$.

(ii) Determine $(\dot{s}_i^{n+\theta})_l$, $i = 2(1)N-1$, $l = 0, 1, 2, \ldots$

(iii) Form a linear system for $(\underline{a}^{n+1})_l$.

(iv) Solve the system for $(\underline{a}^{n+1})_l$.

(v) Investigate the convergence of the iteration.

(vi) If necessary, obtain $(\dot{s}_N^{n+\theta})_{l+1}$ and return to (ii), with l replaced by $l+1$.

Owing to the negligible initial velocity of the moving boundary (see Hansen & Hougaard, 1974), we choose

$$(\dot{s}_N^{\theta})_o = 0 \ , \tag{4.50}$$

in (i). At all other time levels we obtain an initial estimate of the moving boundary velocity as follows. A slight variation of the extrapolation idea, (4.21)-(4.24), of Section 4.1 applied to the new moving boundary amplitude

produces

$$a_N^{n+1} \simeq a_N^n + \Delta t^{n+\frac{1}{2}} \dot{a}^{n+\theta}$$

$$\simeq a_N^n + \Delta t^{n+\frac{1}{2}} \{\dot{a}_N^{n-1+\theta} + \tfrac{1}{2}(\Delta t^{n-\frac{1}{2}} + \Delta t^{n+\frac{1}{2}}) \ddot{a}_N^{n-1+\theta}\}$$

$$\simeq a_N^n + \Delta t^{n+\frac{1}{2}} \left\{\dot{a}_N^{n-1+\theta} + \tfrac{1}{2}(\Delta t^{n-\frac{1}{2}} + \Delta t^{n+\frac{1}{2}}) \dot{a}_N^{n-1+\theta} \frac{d\dot{a}_N}{da_N}\right\}$$

$$\simeq a_N^n + \Delta t^{n+\frac{1}{2}} \dot{a}_N^{n-1+\theta} \left\{1 + \tfrac{1}{2}(\Delta t^{n-\frac{1}{2}} + \Delta t^{n+\frac{1}{2}}) \frac{d\dot{a}_N}{da_N}\right\} , \qquad (4.51)$$

where

$$\Delta t^{n+\frac{1}{2}} = t^{n+1} - t^n , \qquad (4.52)$$

is the difference between the time at levels n and n+1 . The derivative term in (4.51) may be represented via

$$\frac{d\dot{a}_N}{da_N} \simeq [\dot{a}_N^{n-1+\theta} - \dot{a}_{N-1}^{n-1+\theta}]/[a_N^n - a_{N-1}^n] , \qquad (4.53)$$

to yield

$$a_N^{n+1} \simeq a_N^n + \Delta t^{n+\frac{1}{2}} \dot{a}_N^{n-1+\theta} \{1 + \tfrac{1}{2}(\Delta t^{n-\frac{1}{2}} + \Delta t^{n+\frac{1}{2}})[\dot{a}_N^{n-1+\theta} - \dot{a}_{N-1}^{n-1+\theta}]/[a_N^n - a_{N-1}^n]\} , \qquad (4.54)$$

as an approximation to the new amplitude. A central difference form of (4.53), namely

$$\frac{d\dot{a}_{N-1}}{da_{N-1}} \simeq [\dot{a}_N^{n-1+\theta} - \dot{a}_{N-2}^{n-1+\theta}]/[a_N^n - a_{N-2}^n] \ , \qquad (4.55)$$

produces as an estimate of the amplitudal value at the penultimate node

$$a_{N-1}^{n+1} \simeq a_{N-1}^n + \Delta t^{n+\frac{1}{2}} \dot{a}_{N-1}^{n-1+\theta} \{1 + \tfrac{1}{2}(\Delta t^{n-\frac{1}{2}} + \Delta t^{n+\frac{1}{2}})[\dot{a}_N^{n-1+\theta} - \dot{a}_{N-2}^{n-1+\theta}]/[a_N^n - a_{N-2}^n]\} \ . \qquad (4.56)$$

In practice we reduce the danger of inaccuracy due to rounding errors in (4.54) and (4.56) by including the $O[(\Delta t)^2]$ terms only when they are two or more orders of magnitude smaller than the $O[\Delta t]$ ones. The velocities $\dot{a}_{N-2}^{n-1+\theta}$, $\dot{a}_{N-1}^{n-1+\theta}$, $\dot{a}_N^{n-1+\theta}$ are evaluated prior to the n^{th} time level using the Euler formula

$$\dot{a}_J^{n-1+\theta} = [a_J^n - a_J^{n-1}]/\Delta t^{n-\frac{1}{2}} \ , \ J = N-2 \ , \ N-1 \ , \ N \ . \qquad (4.57)$$

The forms (4.54) and (4.56) are substituted into (4.45) to obtain iterates of the boundary velocity through (4.48) and (4.49).

Stage (ii) of the algorithm is provided for via (3.21) with

$$s_1 = 0 \ , \quad \dot{s}_1 = 0 \ , \tag{4.58}$$

and we achieve (iii) using the scheme defined by (3.19). The new amplitudes in Stage (iv) are obtained via the inversion technique outlined in Section 3.2.4.

Having determined the values $(a_i^{n+1})_l$, $i = 1(1)N$, on the l^{th} iteration step at the n^{th} time level, we form a corrected estimate of the moving boundary velocity $(\dot{s}_N^{n+\theta})_l^c$, using (4.49) and (4.45), (4.48) with the amplitudes of time level n+1 represented by the extrapolated estimates. Convergence is then investigated numerically via

$$|(\dot{s}_N^{n+\theta})_l - (\dot{s}_N^{n+\theta})_l^c| < \epsilon \ |(\dot{s}_N^{n+\theta})_l| \ , \tag{4.59}$$

where ϵ is the iteration tolerance. If (4.59) is not satisfied, then a further estimate for the velocity is provided for in Stage (iv) by

$$(\dot{s}_N^{n+\theta})_{l+1} = \omega(\dot{s}_N^{n+\theta})_l + [1 - \omega](\dot{s}_N^{n+\theta})_l^c \ , \tag{4.60}$$

where ω is a relaxation parameter. In practice, at most two iterations are required with the choice

$$\epsilon = \tfrac{1}{2} \times 10^{-3} , \quad \omega = \tfrac{1}{2} , \tag{4.61}$$

and these occur only in the latter stages of the duration of the absorption/diffusion process.

Consider now the special case of $\theta = 0$. We may then formulate our problem in terms of the variables $\dot{a}_i$, $i = 1(1)N$, and $\dot{s}_N$, using $N-1$ equations of the type (3.14) for $\dot{a}_i$, $i = 1(1)N-1$, equation (4.41) for $\dot{s}_N$, while that for $\dot{a}_N$ is obtained by differentiating (4.39), and is

$$\dot{a}_{N-1} + 5\dot{a}_N = 0 . \tag{4.62}$$

The constrained nodal motion idea, (3.21), enables us to express the system in the form

$$\tilde{A}\underline{\dot{y}} = \underline{r} , \tag{4.63}$$

where $\tilde{A}$ is an upper Hessenberg matrix with non-zero entries indicated in Figure 8,

$$\dot{\underline{Y}} = [\dot{a}_1 \ . \ \dot{a}_2 \ . \ \ldots \ . \ \dot{a}_N \ ; \ \dot{s}_N]^T \ . \qquad (4.64)$$

and $\underline{r}$ is a vector of known values. If we

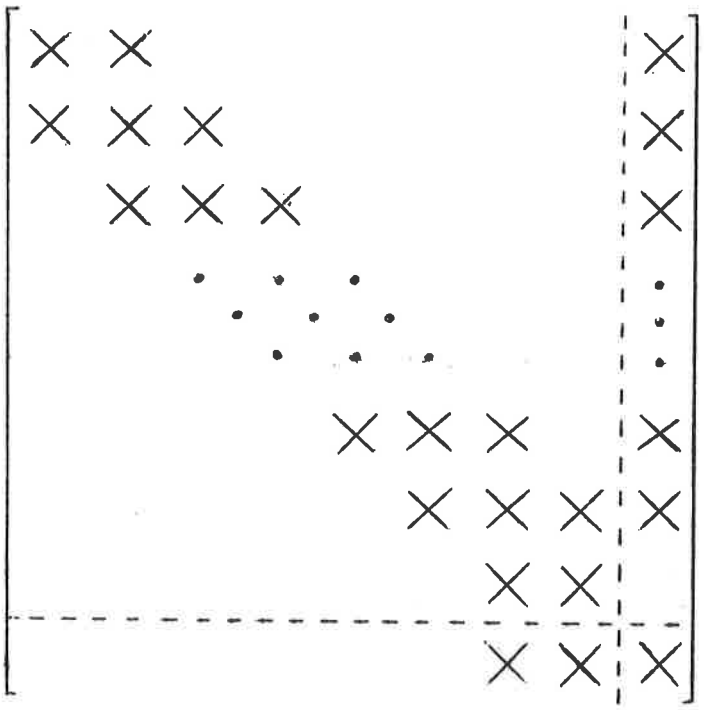

Figure 8

partition $\tilde{A}$ into the form suggested by Figure 8, namely

$$\tilde{A} = \begin{bmatrix} A & \underline{b} \\ \underline{c}^T & d \end{bmatrix} , \tag{4.65}$$

then (4.63) may be expressed as

$$\begin{bmatrix} A & \underline{b} \\ \underline{c}^T & d \end{bmatrix} \begin{bmatrix} \dot{\underline{a}} \\ \dot{s}_N \end{bmatrix} \begin{bmatrix} \underline{r}_a \\ r_s \end{bmatrix} , \tag{4.66}$$

where $\underline{r}_a$ and r_s are the right-hand parts corresponding to the $\dot{\underline{a}}$ and $\dot{s}_N$ equations, respectively. An expansion of the system (4.66) yields

$$\left.\begin{aligned} A\dot{\underline{a}} + \dot{s}_N\underline{b} &= \underline{r}_a \\ \underline{c}^T\dot{\underline{a}} + \dot{s}_N d &= r_s \end{aligned}\right\} , \tag{4.67}$$

the solution of which is given by

$$\left.\begin{aligned} &\text{(i)} \quad \dot{s}_N = [r_s - \underline{c}^T A^{-1}\underline{r}_a]/[d - \underline{c}^T A^{-1}\underline{b}] \\ &\text{(ii)} \quad \dot{\underline{a}} = A^{-1}[\underline{r}_a - \dot{s}_N\underline{b}] \end{aligned}\right\} . \tag{4.68}$$

Another possible method of inverting (4.63) is to reduce the system to upper-triangular form and then to back-substitute for the solution. We do not consider these explicit techniques further in this report.

As t approaches t_2, the time at which zero oxygen remains, the velocity of the moving boundary becomes very large in magnitude. For this reason we restrict the time increment in order to preserve accuracy of the numerical solution. At each time level the difference between the new and present positions of the moving boundary is not allowed to exceed a given multiple of the present one; i.e,

$$|s_N^{n+1} - s_N^n| \leq \phi\, s_N^n \,. \tag{4.69}$$

A Taylor expansion of (4.69), based on the idea of (4.54), yields

$$\Delta t^{n+\frac{1}{2}} \leq \phi\, s_N^n / |\dot{s}_N^{n-1+\theta}| \,, \tag{4.70}$$

to first order in Δt. We take the number of elements into consideration by choosing

$$\phi = \chi/[N-1] \,, \tag{4.71}$$

where χ is a specified accuracy, given by

$$\chi = 0.1 \ , \tag{4.72}$$

for a 10% level. The time increment at each time level is prescribed in accordance with the accuracy citerion, (4.70)-(4.72), and that for stability in Section 3.3.1.

5. Presentation and Analysis of Results

In the ensuing subsections we present and discuss the numerical and graphical results of the test problems of Section 2. In each case numerical results are tabulated with 11, 21 and 41 nodes, but all graphical output contains 21 nodes.

The implicitness parameter θ is given by

$$\theta = \tfrac{1}{2} \tag{5.1}$$

in all runs, thus yielding unconditionally stable schemes according to the analysis of Section 3.3.1. The time increment, which is unrestricted in the case (5.1), is taken to be Δt_{max}, where

$$\Delta t_{max} = 10^{-4} . \tag{5.2}$$

The local truncation error analysis of Section 3.3.2 using (5.1) yields a numerical scheme which is second order accurate both in space and time.

5.1 Results for Problem 1

The numerical solution of the One-phase Stefan Problem

(defined by (2.1)-(2.4)) is initiated at time t_0 (given by (4.5)) using the start-up solution (4.2) and run to final times of 1 and 5 non-dimensional units.

Figures 9 and 10 show the variation of the temperature in the water region at times 0.1(0.1)1.0 and 1.0(1.0)5.0 respectively. The "⅄" symbols denote the water-ice interface positions, the solid lines represent the exact solutions, and the heavy dots are the numerical values. In Figure 9 we see the early linear-like behaviour in the expanding water region and the effect of the Neumann boundary condition (2.2) is clearly visible in the rapidly changing solutions of Figure 10.

Tables 1 and 2 contain the exact positions of the moving boundary and the exact temperatures at the fixed left-hand boundary, respectively, at selected times, together with the relative percentage errors (calculated by dividing the deviation of the numerical values from the exact ones by the exact values and then multiplying by one hundred). In all cases the intial errors, which are due to the implementation of (4.5) in the start-up solution (4.2), decrease in magnitude with time for each fixed number of nodes to a minimum value and then increase. The errors (with a few exceptions up until a time of 1, and none afterwards) reduce

on increasing the number of nodes for a fixed value of time. An order of convergence greater than two is apparent in space in both the moving boundary position and fixed boundary temperature after a time of 1 non-dimensional unit; this rate is not apparent before this time owing to the extreme accuracy of the results - possibly due to the effectiveness of the special treatment in Section 4.1 using only small numbers of nodes.

The c.p.u. times on a Norsk-Data Nord 500 mini computer for 11, 21 and 41 nodes are 18, 33 and 63 seconds, respectively, for a final time of one unit, and are 85, 158 and 304 for a value of 5. The computer times therefore increase approximately linearly with the number of nodes.

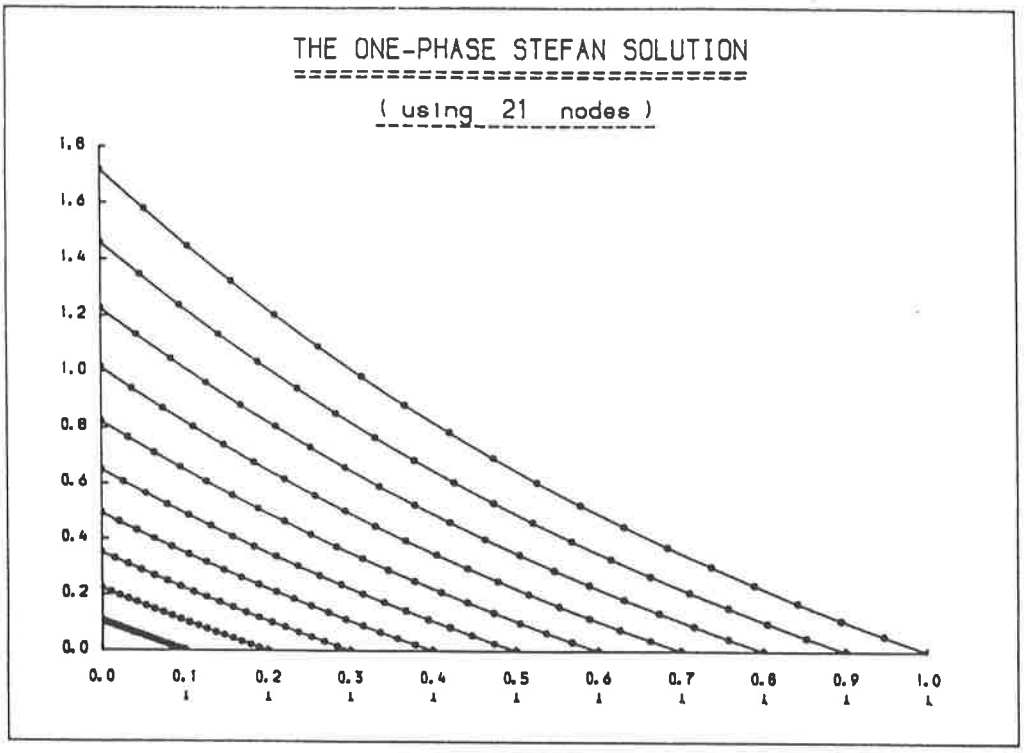

Figure 9

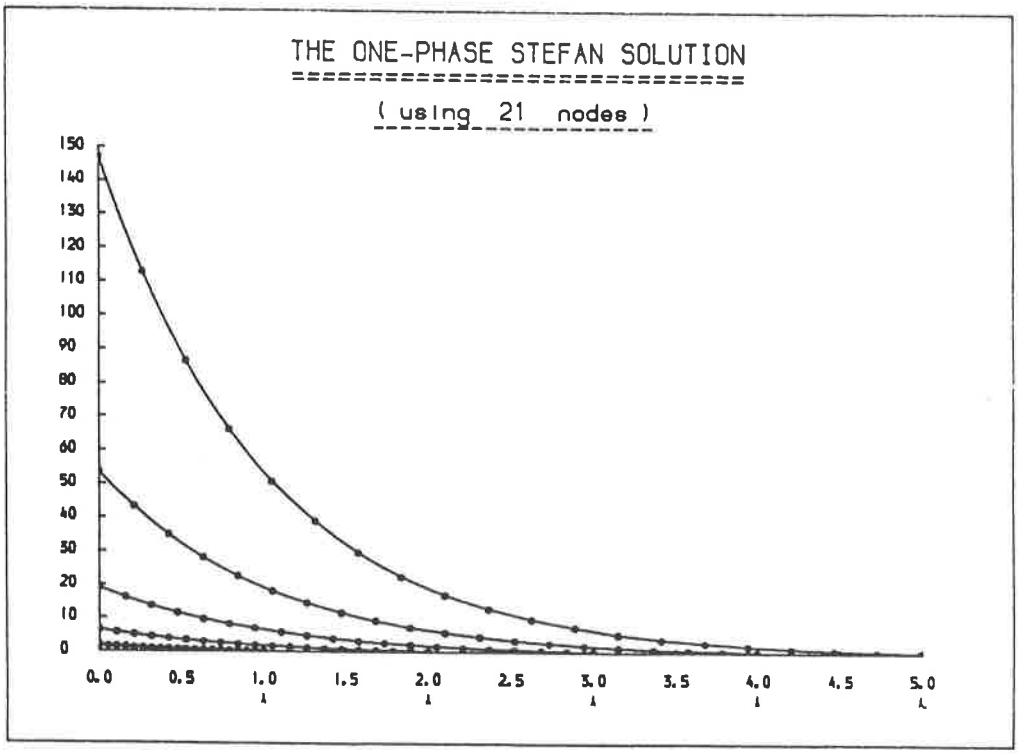

Figure 10

Time	Exact Position	Relative Percentage Error in Position		
		11 Nodes	21 Nodes	41 Nodes
0.01	0.01000	-1.000	-1.000	-1.000
0.10	0.10000	-0.450	-0.430	-0.420
0.20	0.20000	-0.270	-0.255	-0.245
0.30	0.30000	-0.193	-0.180	-0.170
0.40	0.40000	-0.145	-0.135	-0.130
0.50	0.50000	-0.110	-0.108	-0.102
0.60	0.60000	-0.085	-0.088	-0.083
0.70	0.70000	-0.063	-0.073	-0.070
0.80	0.80000	-0.043	-0.060	-0.060
0.90	0.90000	-0.024	-0.050	-0.051
1.00	1.00000	-0.006	-0.041	-0.044
2.00	2.00000	0.171	0.022	-0.009
3.00	3.00000	0.392	0.079	-0.011
4.00	4.00000	0.669	0.145	0.030
5.00	5.00000	1.003	0.222	0.050

Table 1

Problem 1: relative percentage errors in computed moving boundary positions at selected times as compared with the exact values.

Time	Exact Temperature	Relative Percentage Error in Temperature		
		11 Nodes	21 Nodes	41 Nodes
0.01	0.01005	-1.493	-1.493	-1.493
0.10	0.10517	-0.380	-0.361	-0.352
0.20	0.22140	-0.217	-0.203	-0.194
0.30	0.34986	-0.140	-0.134	-0.129
0.40	0.49182	-0.096	-0.098	-0.094
0.50	0.64872	-0.060	-0.071	-0.071
0.60	0.82212	-0.033	-0.054	-0.055
0.70	1.01375	-0.010	-0.039	-0.043
0.80	1.22554	0.012	-0.028	-0.034
0.90	1.45960	0.032	-0.018	-0.027
1.00	1.71828	0.052	-0.010	-0.022
2.00	6.38906	0.259	0.054	0.008
3.00	19.08554	0.535	0.120	0.027
4.00	53.59815	0.896	0.206	0.049
5.00	147.41316	1.344	0.313	0.075

Table 2

Problem 1: relative percentage errors in computed fixed boundary temperatures at selected times as compared with the exact values.

5.2 Results for Problem 2

A typical numerical solution to the Two-phase Stefan Problem, (2.6)-(2.10), may be seen in Figure 11 at times 0.0(0.5)2.5. The variation of the temperature in the expanding ice and diminishing water regions is again represented analytically by the solid lines and numerically by the heavy dots. The right-moving interface nodes (whose positions are again denoted by "人" symbols below the horizontal axis) blend in with their left and right direct neighbours (with the spacing given by (4.26)) to form heavy blobs on the dashed zero temperature line. Although we have simple quadratic solutions in space according to (2.11a), the rapidly accelerating interface position of (2.11b) renders this a difficult problem to treat numerically.

The relative percentage errors of the moving interface position and fixed left- and right-hand boundary temperatures are displayed in tables 3, 4 and 5, respectively, at selected times. We see that the errors in the moving interface positions, which are initially zero, increase with time for a fixed number of nodes; the temperatures at the fixed boundaries, on the other hand, generally decrease from their initial values (obtained via projections in (4.27)) to minima and then increase, like those of Problem 1. The general

trend is for the errors in the moving interface positions and fixed boundary temperatures to decrease as the number of nodes is increased at a fixed time. Quadratic convergence, however, is not exhibited in these results, but may be seen approximately for

$$h_{I-\frac{1}{2}} = 10^{-4} = h_{I+\frac{1}{2}} \tag{5.3}$$

in (4.26a) - although this choice is less robust than that of (4.26b).

Runs with 11, 21 and 41 nodes require 47, 81 and 153 seconds of c.p.u. time on the Nord 500 mini computer, thus illustrating an approximately linear dependence of computer time on the number of nodes.

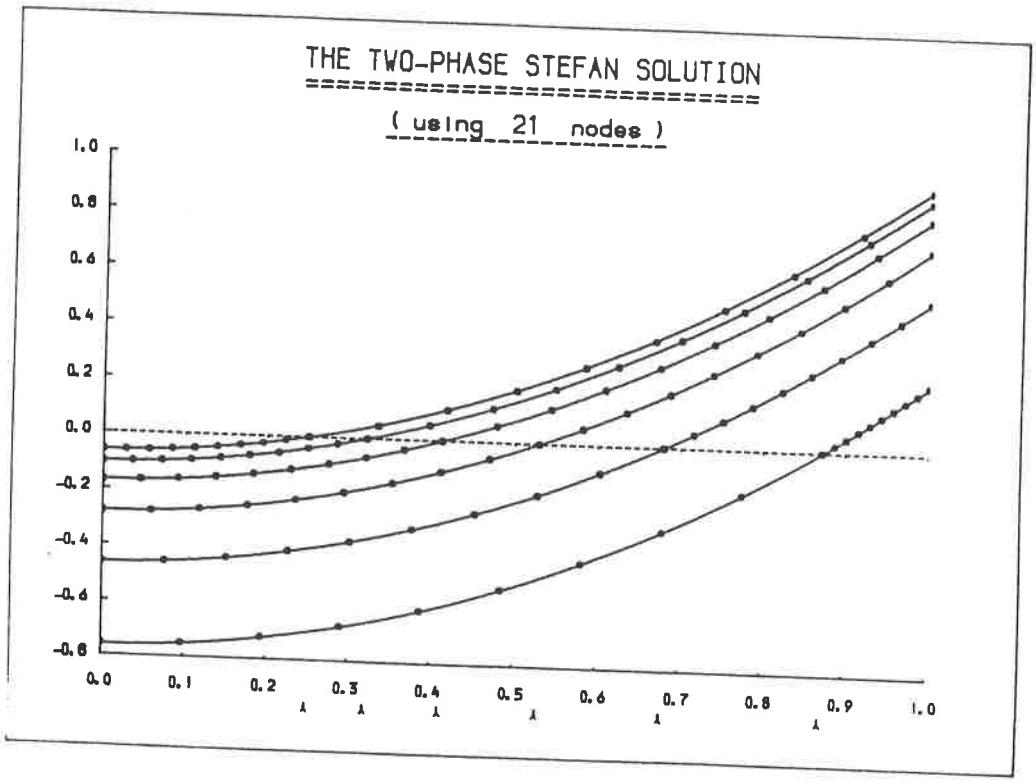
THE TWO-PHASE STEFAN SOLUTION
(using 21 nodes)
1.0
0.8
0.6
0.4
0.2
0.0
-0.2
-0.4
-0.6
-0.8
0.0
0.1
0.2
0.3
0.4
0.5
0.6
0.7
0.8
0.9
1.0
λ

Figure 11

Time	Exact Position	Relative Percentage Error in Position		
		11 Nodes	21 Nodes	41 Nodes
0.0	0.25000	0.000	0.000	0.000
0.5	0.32101	0.072	0.100	0.062
1.0	0.41218	0.184	0.141	0.080
1.5	0.52925	0.246	0.164	0.091
2.0	0.67957	0.243	0.166	0.093
2.5	0.87259	0.185	0.152	0.089

Table 3

Problem 2: relative percentage errors in computed moving interface positions at selected times as compared with the exact values.

Time	Exact Temperature	Relative Percentage Error in Temperature		
		11 Nodes	21 Nodes	41 Nodes
0.0	-0.06250	1.040	0.208	0.048
0.5	-0.10305	0.116	0.194	0.126
1.0	-0.16989	-0.300	-0.259	-0.153
1.5	-0.28011	-0.393	-0.296	-0.171
2.0	-0.46182	-0.353	-0.245	-0.169
2.5	-0.76141	-0.206	-0.244	-0.152

Table 4

Problem 2: relative percentage errors in computed fixed left-hand boundary temperatures at selected times as compared with the exact values.

Time	Exact Temperature	Relative Percentage Error in Temperature		
		11 Nodes	21 Nodes	41 Nodes
0.0	0.93750	1.623	0.124	0.028
0.5	0.89695	0.011	-0.011	-0.009
1.0	0.83011	-0.105	-0.054	-0.028
1.5	0.71989	-0.210	-0.122	-0.065
2.0	0.53818	-0.429	-0.281	-0.156
2.5	0.23859	-1.195	-0.981	-0.578

Table 5

Problem 2: relative percentage errors in computed fixed right-hand boundary temperatures at selected times as compared with the exact values.

5.3 Results for Problem 3

In Figure 12 we see numerical solutions of the Oxygen Diffusion with Absorption Problem (2.13)-(2.16), at times 0.00(0.01)0.19. The solid squares, joined by the linear segments, denote the nodal concentrations and the "⅄" symbols locate the moving boundary. The negligible initial and large final velocities of the boundary are apparent in Figure 13, which displays the variation of the position of the boundary (on the vertical axis) with time.

The convergence parameters ϵ , ω , defined in (4.61), and the constant χ , of (4.72), are implemented in the numerical solutions. Robustness is illustrated by obtaining very infrequent, negligible deviations in the numerical results when ϵ is decreased by two orders of magnitude.

The nature of the problem is such that zero oxygen remains in the tumour tissue after a time t_2 . Values of 0.197050, 0.197424 and 0.197417 for t_2 are obtained with 11, 21 and 41 nodes respectively, thus indicating a final time of about 0.19742 non-dimensional units. This number compares favourably with those of previous workers: 0.1972-0.1977 of Hansen & Hougaard (1974), 0.1973 of Gupta & Kumar (1981) and 0.197434 of Dahmardah & Mayers (1983).

Tables 6 and 7 contain the numerical values for the moving boundary position and the concentration of oxygen at the fixed boundary, respectively, at selected times; also included are the results of Hansen & Hougaard (1974), which are considered to be the most accurate available in the absence of a known analytical solution, for comparison purposes. We see that all sets of results, especially those with 41 nodes, are very comparable to the Hansen & Hougaard (1974) values - and are increasingly so for increasing numbers of nodes at fixed times, in general. Note that the 21 and 41 results are in excellent agreement with each other, particularly in the case of the oxygen concentration at the fixed boundary (the initial values of which are calculated using an L_2 projection of the initial data function (2.16) onto the space of piecewise linear functions), even in the final stages.

The numerical results exhibit an approximately quadratic rate of convergence, both with respect to the Hansen & Hougaard (1974) values and with respect to themselves.

Again, the dependence of c.p.u. time on the number of nodes is linear-like, with times of 7, 13 and 32 seconds for 11, 21 and 41 nodes respectively.

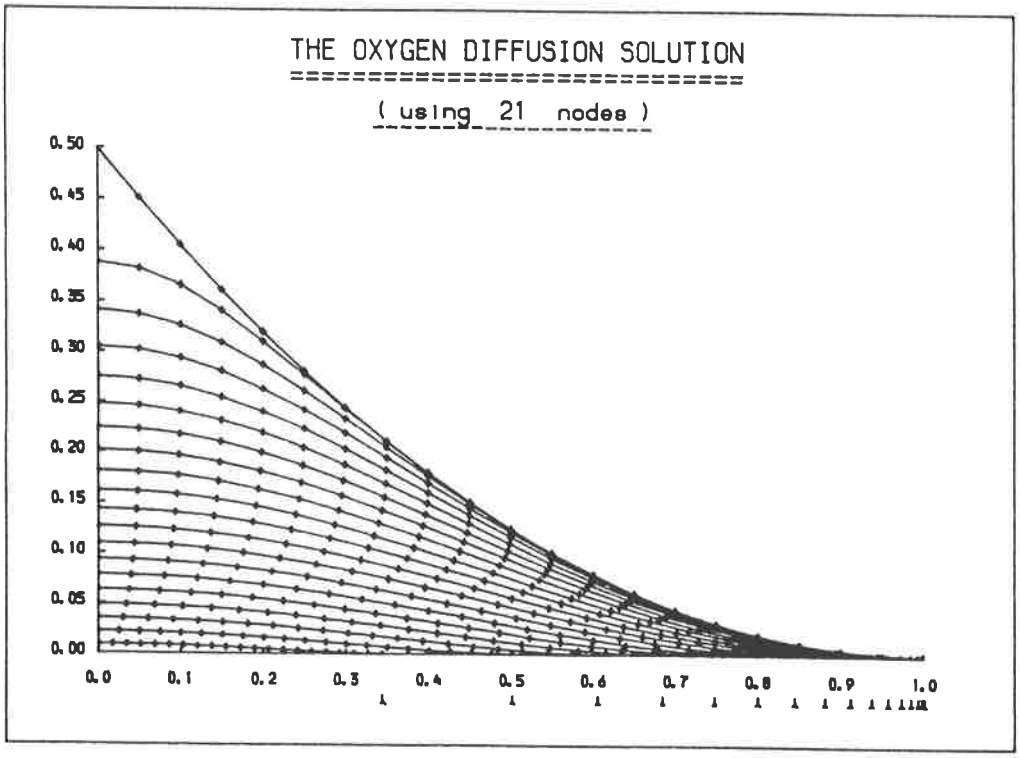

Figure 12

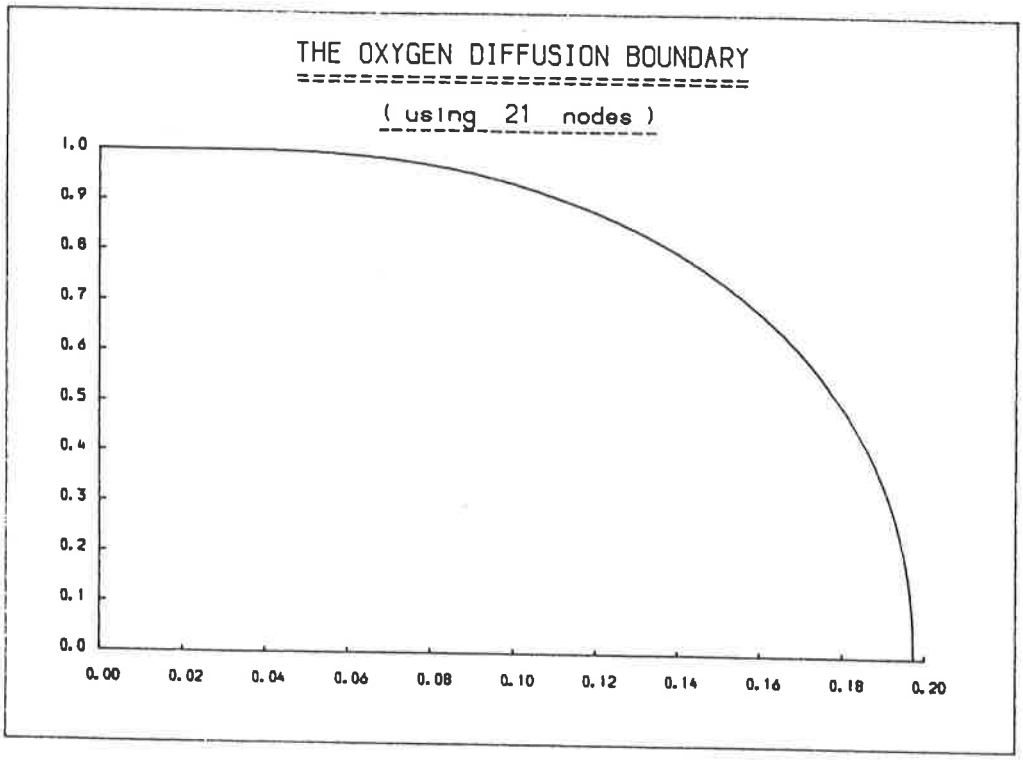

Figure 13

Time	Hansen & Hougaard (1974)	Computed Position		
		11 Nodes	21 Nodes	41 Nodes
0.0000	1.00000	1.00000	1.00000	1.00000
0.0100	1.00000	1.00000	1.00000	1.00000
0.0200	1.00000	1.00000	1.00000	1.00000
0.0300	-	1.00002	0.99995	0.99992
0.0400	0.99918	0.99982	0.99936	0.99923
0.0500	0.99679	0.99823	0.99717	0.99689
0.0600	0.99180	0.99407	0.99239	0.99195
0.0700	-	0.98652	0.98431	0.98372
0.0800	0.97155	0.97510	0.97246	0.97177
0.0900	-	0.95944	0.95649	0.95572
0.1000	0.93501	0.93922	0.93608	0.93526
0.1100	-	0.91403	0.91082	0.90999
0.1200	0.87916	0.88336	0.88022	0.87939
0.1300	-	0.84651	0.84355	0.84277
0.1400	0.79891	0.80243	0.79979	0.79909
0.1500	0.74668	0.74953	0.74739	0.74682
0.1600	0.68337	0.68526	0.68384	0.68345
0.1700	-	0.60508	0.60472	0.60460
0.1800	0.50109	0.49938	0.50072	0.50102
0.1850	0.43341	0.42996	0.43267	0.43318
0.1900	0.34537	0.33900	0.34476	0.34553
0.1950	0.20652	0.19266	0.20713	0.20754
0.1955	0.18708	0.16879	0.18631	0.18630
0.1960	0.16266	0.14056	0.16178	0.16186
0.1965	0.13284	0.10360	0.13223	0.13208
0.1970	0.09175	0.03285	0.09151	0.09109
0.1971	-	-	0.08068	0.07995
0.1972	0.06708	-	0.06763	0.06673
0.1973	-	-	0.05100	0.04962
0.1974	-	-	0.02323	0.01951

Table 6

Problem 3: computed moving boundary positions at selected times as compared with those of Hansen & Hougaard (1974).

Time	Hansen & Hougaard (1974)	Computed Concentration		
		11 Nodes	21 Nodes	41 Nodes
0.0000	0.50000	0.49917	0.49979	0.49995
0.0100	0.38716	0.38876	0.38755	0.38726
0.0200	0.34042	0.34128	0.34063	0.34047
0.0300	-	0.30510	0.30469	0.30459
0.0400	-	0.27468	0.27441	0.27435
0.0500	0.24769	0.24791	0.24774	0.24770
0.0600	0.22361	0.22373	0.22363	0.22361
0.0700	-	0.20150	0.20147	0.20146
0.0800	-	0.18082	0.18084	0.18085
0.0900	-	0.16140	0.16147	0.16148
0.1000	0.14318	0.14303	0.14314	0.14317
0.1100	-	0.12557	0.12572	0.12576
0.1200	0.10913	0.10890	0.10908	0.10912
0.1300	-	0.09291	0.09312	0.09317
0.1400	0.07785	0.07754	0.07778	0.07784
0.1500	0.06308	0.06274	0.06300	0.06307
0.1600	0.04882	0.04845	0.04874	0.04881
0.1700	-	0.03466	0.03497	0.03505
0.1800	0.02178	0.02135	0.02169	0.02177
0.1850	-	0.01489	0.01524	0.01531
0.1900	0.00902	0.00857	0.00896	0.00901
0.1950	0.00288	0.00244	0.00286	0.00287
0.1955	-	0.00183	0.00227	0.00226
0.1960	-	0.00123	0.00167	0.00166
0.1965	-	0.00064	0.00108	0.00107
0.1970	-	0.00006	0.00049	0.00048
0.1971	-	-	0.00038	0.00037
0.1972	-	-	0.00026	0.00025
0.1973	-	-	0.00014	0.00013
0.1974	-	-	0.00003	0.00002

Table 7

Problem 3: computed fixed boundary concentrations at selected times as compared with those of Hansen & Hougaard (1974).

6. Conclusions

We have applied a constrained moving finite element method to three typical one-dimensional moving boundary problems. The method is accurate and numerical results show an approximate second order rate of convergence. The low c.p.u. times, which increase linearly with the number of nodes, indicate a very inexpensive solution technique.

In future work we hope to extend the method to solve the corresponding two-dimensional versions of the problems considered here.

Acknowledgements

The author would like to express gratitude for the continuous and expert supervision of Dr. M.J. Baines and acknowledge the useful suggestions of Dr. C.P. Please, now of the University of Southampton, throughout the duration of this project, the funding of which was provided for by an SERC CASE Studentship in association with GEC.

Appendix

We describe here an approximate technique for imposing a Dirichlet condition of the form of (3.13) weakly at a fixed boundary, which for simplicity is taken to be at $x = 0$.

If we assume that the true solution can be adequately represented in the first element, $[s_1, s_2]$, by a quadratic function q , defined by (4.7), then the analysis (4.9)-(4.12) yields

$$5a_1 + a_2 = 6q_1 + h_2\tilde{q}_1 \ , \qquad (A.1)$$

where a_1 and a_2 are the numerical amplitudes at the nodes s_1, s_2 , respectively, and

$$\left.\begin{aligned} q_1 &= q(s_1) \\ \tilde{q}_1 &= q'(s_1) \end{aligned}\right\} \ . \qquad (A.2)$$

For a Dirichlet condition such as (3.13) we replace $u(s_1)$ by $q(s_1)$ and re-write (A.1) as

$$\tilde{q}_1 = \{a_1 + 5a_2 - 6q_1\}/h_2 \ , \qquad (A.3)$$

which is used as an approximation to $u_x(s_1)$. Thus, with the assumption of an asymptotic functional form close to the boundary, the Dirichlet Condition (3.13) may be imposed as a Neumann one and entered into the weak form of the differential equation.

References

ATTHEY, D.R. (1974) J. Inst. Math. Appl. 13, 353-66.

BAINES, M.J. (1985) Numer. Anal. Report 9/85, Dept. of Maths., Univ. of Reading.

BELL, G.E. (1982) Int. J. Heat Mass Transfer 25, 587-9.

BONACINI, C., COMINI, G., FASANO, A. & PRIMICERIO, M. (1973) Int. J. Heat Mass Transfer 16, 1825-32.

BONNEROT, R. & JAMET, P. (1979) J. Comput. Phys. 32, 145-67.

CAREY, G.F. & HUNG, T.D. (1985) SIAM J. Numer. Anal. 22(5), 1028-40.

CHERNOUSKO, F.L. (1970) Int. Chem. Engng. 10(1), 42-8.

CIAVALDINI, J.F. (1975) SIAM J. Numer. Anal. 12, 464-87.

CRANK, J. (1984) 'Free and Moving Boundary Problems', Clarendon Press, Oxford.

CRANK, J. & GUPTA, R.S. (1972a) J. Inst. Math. Appl. 10, 19-33.

CRANK, J. & GUPTA, R.S. (1972b) J. Inst. Math. Appl. 10, 296-304.

CRANK, J. & PHAHLE, R.D. (1973) Bull. Inst. Math. Appl. 9, 12-4.

DAHMARDAH, H.O. & MAYERS, D.F. (1983) IMA J. Numer. Anal. 3, 81-5.

DIX, R.C. & CIZEK, J. (1970) In 'Heat Transfer Vol. I, 4th. Int. Heat Transfer Conf., Paris, Versailles', Elsevier, Amsterdam.

DOUGLAS, J. & GALLIE, J.M. (1955) Duke Math. J. 22, 557-71.

EYRES, N.R., HARTREE, D.R., INGHAM, J., JACKSON, R., SARJANT, R.J. & WAGSTAFF, S.M. (1946) Phil. Trans. R. Soc. A240, 1-57.

FERRISS, D.H. & HILL, S. (1974) Report NAC45, National Physical Laboratory, Teddington.

FURZELAND, R.M. (1980) J. Inst. Math. Appl. 26, 411-29.

GUPTA, R.S. & KUMAR, D. (1980) Comput. Meth. Appl. Mech. Engng., 23, 101-9.

GUPTA, R.S. & KUMAR, D. (1981) Int. J. Heat Mass Transfer 24, 251-9.

HANSEN, E.B. & HOUGAARD, P. (1974) J. Inst. Math. Appl. 13, 385-98.

HOFFMAN, K.-H. (ed.) (1977) Freie Universität (Berlin) 'Fachbereich Mathematik' Vols. I-III.

JOHNSON, I.W. (1984) Numer. Anal. Report 3/84, Univ. of Reading.

LANDAU, H.G. (1950) Q. Appl. Math. 8, 81-94.

LYNCH, D.R. (1982) J. Comput. Phys. 47, 387-411.

MILLER, J.V., MORTON, K.W. & BAINES, M.J. (1978) J. Inst. Math. Appl. 22, 467-77.

MILLER, K. (1981) SIAM J. Numer. Anal. 18(6), 1033-57.

MILLER, K. & MILLER, R.N. (1981) SIAM J. Numer. Anal. 18(6), 1019-32.

MOODY, R.O. (1985) Numer. Anal. Report 17/85, Dept. of Maths., Univ. of Reading.

MORTON, K.W. (1983) In 'Proc. Fifth G.A.M.M. Conf. on Numerical Methods in Fluid Dynamics' (eds. Pandolfi, M. & Piva, R.), F. Vieweg & Sohn, Wiesbaden, 243-50.

MUELLER, A. (1983) Ph.D. Thesis, Univ. of Texas at Austin.

MURRAY, W.D. & LANDIS, F. (1959) J. Heat Transfer, Trans. ASME, (c)81, 106-12.

NITSCHE, J.A. (1980) In 'Free Boundary Problems Vols. I and II. Proceedings of a seminar in Pavia (1979)' (ed. Magenes, E.), Instituto Nazionale di Alta Matematica Francesco Severi, Rome, Vol. I, 277-318.

O'NEILL, K. & LYNCH, D.R. (1981) In 'Numerical Methods in Heat Transfer' (eds. Lewis, R.W., Morgan, K. & Zienkiewicz, O.C.), Wiley, New York.

RICHTMYER, R.D. & MORTON, K.W. (1967) 'Difference Methods for Initial-value Problems', Interscience, New York.

STEFAN, J. (1889a) Sber. Akad. Wiss. Wien. 98, 473-84.

STEFAN, J. (1889b) Sber. Akad. Wiss. Wien. 98, 965-83.

STEFAN, J. (1891) Ann. Phys. U. Chem. 42, 269-86.

VOLLER, V.R. & CROSS, M. (1981) Int. J. Heat Mass Transfer 24, 545-56.

WATHEN, A.J. & BAINES, M.J. (1985) IMA J. Numer. Anal. 5, 161-82.